





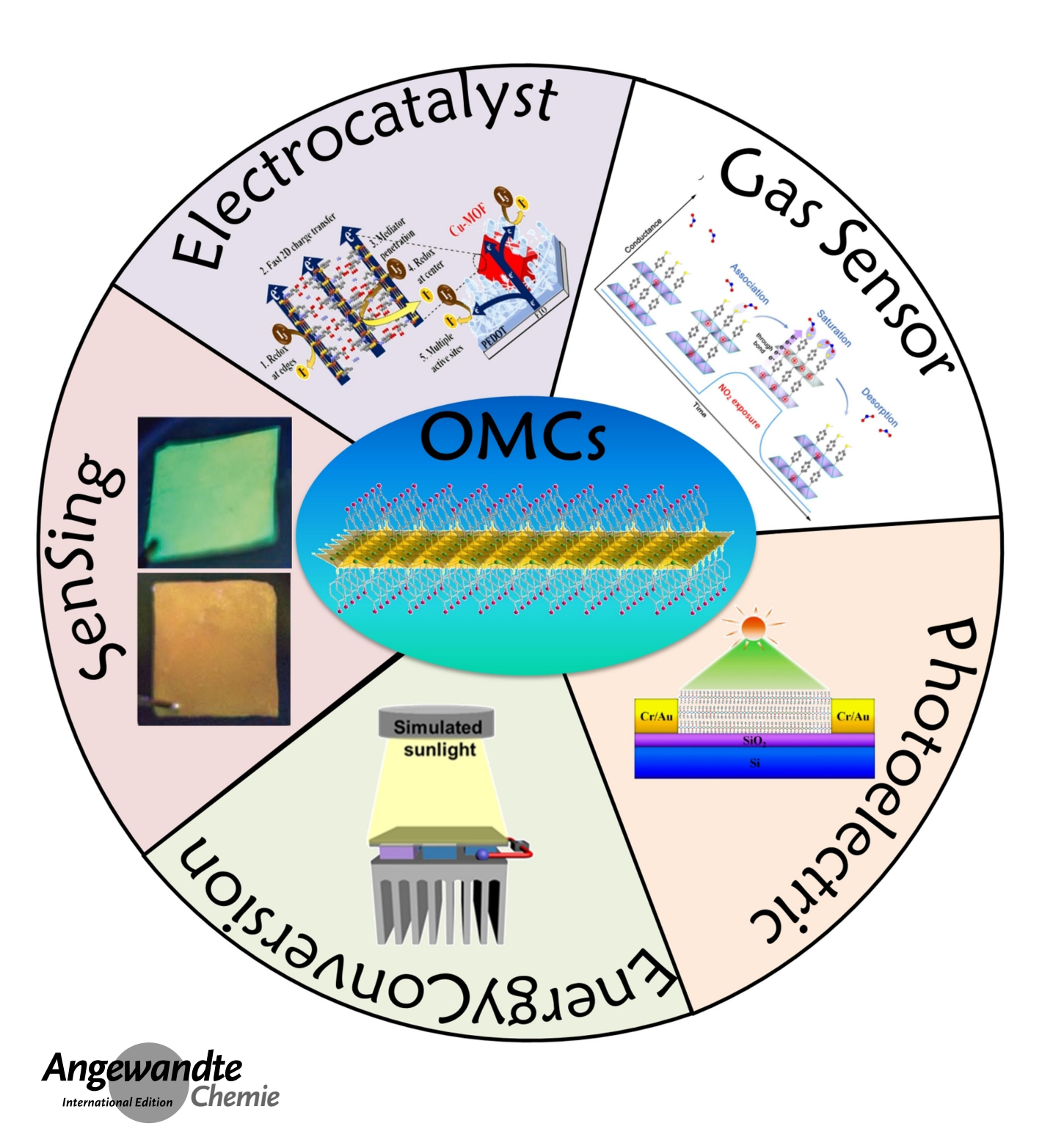
2D Materials

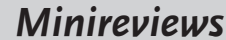
How to cite:

International Edition: doi.org/10.1002/anie.202203151
German Edition: doi.org/10.1002/ange.202203151

# Layered Organic Metal Chalcogenides (OMCs): From Bulk to Two-Dimensional Materials

Guan-E Wang, ShaoZhen Luo, Tuo Di, ZhiHua Fu, and Gang Xu\*









Abstract: The modification of inorganic two-dimensional (2D) materials with organic functional motifs is in high demand for the optimization of their properties, but it is still a daunting challenge. Organic metal chalcogenides (OMCs) are a type of newly emerging 2D materials, with metal chalcogenide layers covalently anchored by long-range ordered organic functional motifs, these materials are extremely desirable but impossible to realize by traditional methods. Both the inorganic layer and organic functional motifs of OMCs are highly designable and thus provide this type of 2D materials with enormous variety in terms of their structure and properties. This Minireview aims to review the latest developments in OMCs and their bulk precursors. Firstly, the structure types of the bulk precursors for OMCs are introduced. Second, the synthesis and applications of OMC 2D materials in photoelectricity, catalysis, sensors, and energy transfer are explored. Finally, the challenges and perspectives for future research on OMCs are discussed.

### 1. Introduction of Two-Dimensional OMCs and Their Bulk Precursors

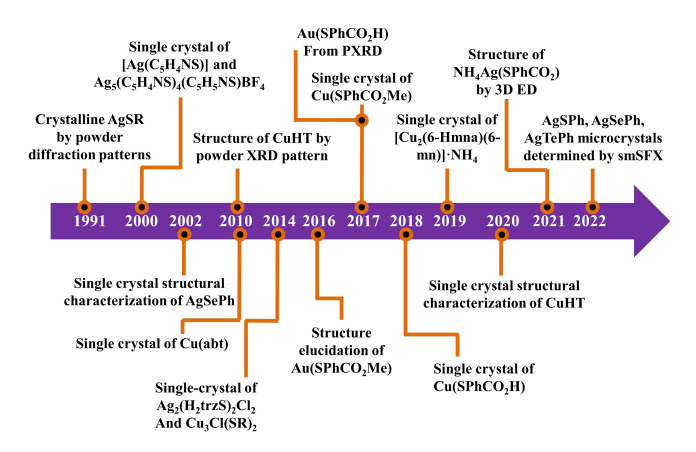
Intensive efforts have been directed to the synthesis of ultrathin single-layer or few-layered (defined as two-dimensional (2D)) materials because they display unique physical, chemical, and electronic properties compared with their bulk counterparts.[1] Organic functional molecules grafted onto the surface of 2D materials by covalent bonding can further modulate the band gap of the original material, promote its dispersion in solvent, increase light absorption, and improve its affinity to target analytes. [2] In the past decades, dramatic achievements have been made in the post-modification of organic functional groups on the already exfoliated nanosheet (Exfoliation then Modification (E-M) strategy). The E-M strategy often requires violent harsh physical and chemical treatments that destroy the integrated structure of the nanosheet. Meanwhile, the reported post-modification has low efficiency and only a small proportion of the 2D surface can be modified. As a result, the organic groups cannot be homogeneously distributed over the whole surface of the 2D nanosheet, thereby impeding the application of these materials. Furthermore, these materials have no definite structure, which is not conducive to the analysis of their structure-activity relationship.

are 2D organic metal chalcogenides (OMCs).[3] Compared with well-known 2D materials such as graphene and transition metal dichalcogenides (TMDs), OMCs possess a very unique structure. The inorganic lamellar layer is covered by organic molecules that are attached through

An emerging family within this broader class of materials covalent interactions, and the OMCs are further held structure in bulk precursors. The inorganic layer is isolated by organic moieties to form a multi-quantum wells.[4] Covalent interactions between organic and inorganic components makes OMCs dispersible in various solvents and endows them with unique electronic structures that can be adjusted by organic modification. Furthermore, owing to the variability of inorganic layers and organic molecules, these materials can be modulated in terms of layer number, layer width, composition, and structure types that offer the possibility of tuning their absorption, luminescence, band gap, carrier type, carrier mobility, etc. Thus, OMCs can be potentially applied to opto/electronics, energy storage, and catalysis. The study of the bulk precursors for OMCs has a long history, [5] thereby laying a solid material foundation for further delamination (Scheme 1).

together by van der Waals forces to form a superlattice

Considering the unique structural characteristics of these materials, the surface of the inorganic layer can be premodified by the attachment of organic functional molecules through coordination chemistry self-assembly. Exfoliation of such materials can result in monolayer or few-layered nanosheets fully covered with organic functional molecules (Modification then Exfoliation (M–E) strategy (Figure 1). These OMCs feature unique advantages: 1) Benefitting from



**Scheme 1.** Timeline of important events in the development of OMCs. AgSR,  $^{[6]}$  single crystals of [Ag(C<sub>5</sub>H<sub>4</sub>NS)] and Ag<sub>5</sub>(C<sub>5</sub>H<sub>4</sub>NS)<sub>4</sub>-(C<sub>5</sub>H<sub>5</sub>NS)BF<sub>4</sub>, [7] AgSePh, [8] CuHT, [9] Cu(abt), [10] single crystals of Ag<sub>2</sub>- $(H_2 trzS)_2 Cl_2^{[11]}$  and  $Cu_3 Cl(SR)_2$ , [12] [Au(SPhCO<sub>2</sub>Me)]<sub>n</sub>, [13] single crystals of Cu(SPhCO<sub>2</sub>Me), [14] Cu(SPhCO<sub>2</sub>H), [15] and [Cu<sub>2</sub>(6-Hmna) (6-mn)]·NH<sub>4</sub>, [16] single crystal structure of CuHT,[3] NH<sub>4</sub>Ag(SPhCO<sub>2</sub>),[17] AgSPh, AgSePh, and AgTePh microcrystals.[18]

[\*] Prof. G.-E Wang, S. Luo, T. Di, Z. Fu, Prof. G. Xu State Key Laboratory of Structural Chemistry Fujian Institute of Research on the Structure of Matter Chinese Academy of Sciences (CAS) 155 Yanggiao Road West, Fuzhou, Fujian, 350002 (China) E-mail: gxu@fjirsm.ac.cn

S. Luo

College of Chemistry and Materials Science Fuiian Normal University Fuzhou, Fujian 350007 (P. R. China)

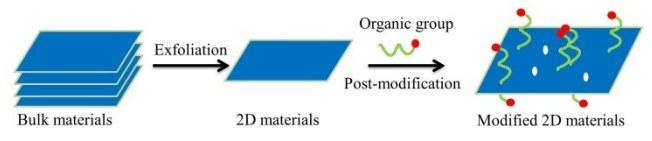
Prof. G. Xu

Fujian Science & Technology Innovation Laboratory for Optoelectronic Information of China Fuzhou, Fujian 350108 (China)





a) Exfoliation and then organic modification (E-M)



b) Organic modification and then exfoliation (M-E)

Organic thiophene Heli-assembly Exfoliation

Metal ion

Well-defined structure

Figure 1. Comparison of the two synthetic strategies for functionalized 2D materials.

√ Periodically arranged functional groups
 √ Adjustable functional group

coordination chemistry, these OMCs possess great structural diversity. 2) Organic functional groups have been introduced

during the synthesis of bulk precursor; thus, complex organic post-modification is no longer needed. 3) Organic functional groups are periodically arranged on the inorganic metal-chalcogen layer, which provides more specific active sites. 4) The adjacent layers are connected by van der Waals interactions in the bulk precursor. The exfoliation conditions are mild, thereby reducing the defects on the surface of OMCs.

Recently, studies on OMCs have been attracting increasing attention. Reviewing the synthesis, structures, exfoliation methods, and applications of OMCs is significant in providing insights into the rational design, preparation, and functional exploitation of these materials. In OMCs, the metal coordinates with the organic sulfur to form a two-dimensional layered structure, and the sulfur further links to the organic group through covalent bonds to form a functional group layer. Therefore, the organic part plays an important role in OMCs, and we just focus on this system here. Other material systems, such as organic–inorganic networks of hybrid chalcogenides, where inorganic sulfur or selenium coordinates with metals to form two-dimensional layered structures and is further sliced by organic amine, [19] will not



Guan-E Wang earned her PhD in 2013 from Fujian Institute of Research on the Structure of Matter, Chinese Academy of Science (FJIRSM, CAS). She is currently a professor at FJIRSM. Her research focuses on porous conductive inorganic-organic hybrids.



Gang Xu received his PhD in 2008 from Fujian Institute of Research on the Structure of Matter (FJIRSM), CAS. He worked as postdoctoral fellow at COS-DAF in City University of Hong Kong (Hong Kong), University of Regensburg (Alexander von Humboldt fellowship, Germany) and Kyoto University (JSPS fellowship, Japan). In 2013, he joined FJIRSM and conducted independent research as a Pl. His research interests are conductive coordination polymers, thinfilm preparation, and electric devices.



Tuo Di is a PhD candidate under the supervision of Prof. Hiroshi Kitagawa of the Department of Chemistry, Faculty of Science, Kyoto University (Japan) and Prof. Gang Xu of Fujian Institute of Research on the Structure of Matter, Chinese Academy of Sciences. His main research interests are porous coordination polymers and proton conduction.



Zhihua Fu is an assistant researcher at the Fujian Institute of the Structure of Matter. He received his PhD in organic chemistry from Zhengzhou University in 2014 under the supervision of Prof. Tiesheng Li. From 2017 to 2019, he was engaged in postdoctoral research at the Institute of Functional Interfaces, Karlsruhe Institute of Technology (Germany) under the supervision of Prof. Christof Wöll. His research interests focus on the development of functional conductive materials and their applications.



Shao-Zhen Luo received her undergraduate degree from Hebei Normal University in 2020. She is currently pursuing postgraduate studies at Fujian Normal University and Fujian Institute of Research on the Structure of Matter (mentor: Guan-E Wang). Her research focuses on synthesizing and studying the performance of organic metal chalcogenides.





be included here. This Review comprises four parts. The first part presents the structure types of the potential bulk precursors for OMCs. In the second part, the methods for the synthesis of the nanosheets (thick flakes with thickness of tens to hundreds nanometers) and OMCs (single layer or a few-layers with thickness of less than 5 nm) are summarized. The applications of nanosheets and OMCs as sensors and in solar energy conversion and electrocatalysts etc. are reviewed in the third part. Finally, the challenges and prospects for the further development of OMCs will also be summarized.

### 2. Structures of the Bulk Precursors for OMCs

OMCs have the general formula of MSR  $(M=Cu^+, Ag^+,$ and Au<sup>+</sup> etc.; R=alkyl chain) or M(SPhX) (HSPh= benzenethiol, X = functional group; H, -COOH, -F, -OCH<sub>3</sub>, -OH, -NH<sub>2</sub> etc.), where S can be superseded by Se or Te. The coordination reaction between S (Se or Te) and metals ions occurs very quickly, making characterization difficult. The samples are polycrystalline with low symmetry and serious radiation sensitivity, thereby not suitable for standard single-crystal X-ray diffraction (SC-XRD) analysis. At present, most of these structures are fitted by powder diffraction results. One way to solve this problem is by using 3D electron diffraction (ED).<sup>[17]</sup> A crystal that is regarded as a powder in X-ray crystallography can be treated as a single crystal by the 3D ED method due to the strong interaction between electrons and matter. The structure of NH<sub>4</sub>Ag-(SPhCO<sub>2</sub>) (HSPhCO<sub>2</sub>H = para-mercaptobenzoic acid) was resolved by this method. [17] Recently, Hohman et al. exploited a new small-molecule serial femtosecond X-ray crystallography (smSFX) technique to determine the crystal structures of microcrystals.<sup>[18]</sup> Thousands of randomly oriented diffraction patterns were obtained from microcrystalline suspensions subjected to X-ray free-electron laser radiation. After aggregating the spot-finding results into high-resolution powder diffractograms, the unit cells parameters can be indexed. The resulting datasets can be resolved and refined for single-crystal diffraction data using standard tools after indexing the sparse serial patterns by a graph theory approach. The structures of microcrystals mithrene (AgSePh), thiorene (AgSPh), and tethrene (AgTePh) were resolved by this method, whereby the structures of AgSPh and AgTePh had never been reported before.

#### 2.1. Two-Dimensional OMCs Based on MS, Layers

The layer structure of AgSR ( $R = (CH_2)_2CH_3$ ,  $(CH_2)_3CH_3$ ,  $(CH_2)_3CH_3$ ,  $(CH_2)_3CH_3$ ,  $(CH_2)_7CH_3$ ,  $C_6H_5$ ,  $C_6H_4$ -4-F,  $C_6H_4$ -4-Cl,  $C_6H_4$ -4-Br,  $C_6H_4$ -4-CH<sub>3</sub>,  $C_6H_4$ -4-OCH<sub>3</sub>) were reported as early as 1991. [6] From diffraction patterns, the structures of these compounds can be interpreted as regularly stacked AgS layers, and the interlayer lattice dimension is longer than the intralayer two-dimensional lattice. The spacings between two layers are highly related to the length of the alkyl chains.

The definite structure of Cu-based OMCs (copper(I) 4-hydroxythiophenolate (CuHT)) first reported by Che et al. was resolved by powder XRD data. The single-crystal structure of this compound was first resolved by Xu et al. The structures obtained by these two methods are nearly the same. As reported, three  $\mu_3$ -bridging S atoms coordinate to one Cu atom to construct a slightly distorted trigonal-planar geometry. Each S atom also connects to three Cu atoms to form a Cu<sub>3</sub>S<sub>3</sub> hexagon. An infinite honeycomb-like layer network is formed by these interconnecting Cu<sub>3</sub>S<sub>3</sub> hexagons. 4-Hydroxyphenyl moieties covered both sides of this layer (Figure 2). The –OH functional group extending out from the inorganic layer can be replaced by other functional groups, such as –NH<sub>2</sub>, –OCH<sub>3</sub>, –F, or –CO<sub>2</sub>H, and the center metal can be replaced by Ag or Au. [3]

The second structure in the family of copper OMCs, Cu(SPhCO<sub>2</sub>Me),<sup>[14]</sup> was obtained from a redox reaction between Cu(NO<sub>3</sub>)<sub>2</sub> and *p*-HSPhCO<sub>2</sub>Me under solvothermal conditions. The lamellar structure of Cu(SPhCO<sub>2</sub>Me) is quite similar to that of CuHT, and the only difference is that there are no hydrogen bond interactions between the layers for the esterification of the terminal carboxyl groups in Cu(SPhCO<sub>2</sub>Me) (Figure 3).

Cu(SPhCO<sub>2</sub>H) shows a structure (Figure 4) similar to those of CuHT and Cu(SPhCO<sub>2</sub>Me). Owing to the presence of carboxylic acids, dimeric hydrogen bond interactions are found between two neighboring layers. The presence of hydrogen bond interactions results in the formation of distorted [Cu<sub>3</sub>S<sub>3</sub>] hexagons, whereas the

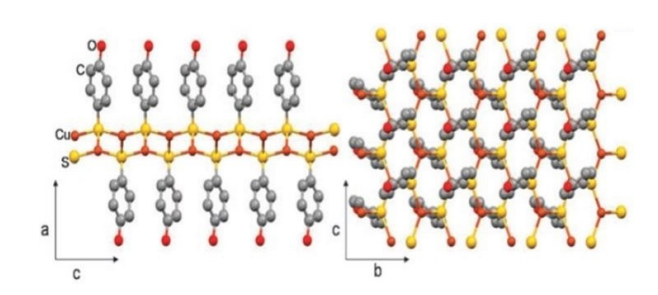


Figure 2. Side view and top views of the two-dimensional CuHT structure. [9] Copyright 2010 Royal Society of Chemistry.

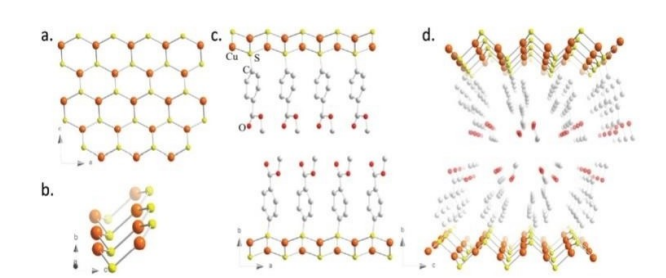
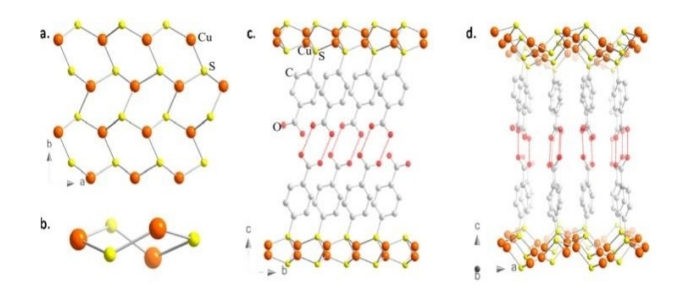


Figure 3. Structure of  $Cu(SPhCO_2Me)$ . a) Inorganic sheet of  $Cu_3S_3$  hexagons on the ac plane. b) Half-chair conformation of  $Cu_3S_3$  hexagons. c) Structure of  $Cu(SPhCO_2Me)$  viewed on the ab plane. d) Central projection structure of  $Cu(SPhCO_2Me)$  along the a axis. [14] Copyright 2017 Royal Society of Chemistry.







**Figure 4.** Structure of Cu(SPhCO<sub>2</sub>H): a) Cu<sub>3</sub>S<sub>3</sub> hexagons. b) Cu<sub>3</sub>S<sub>3</sub> cycle in the inorganic layer. The lamellar structure viewed along the a (c) and b (d) axis, respectively.<sup>[15]</sup> Copyright 2018 Royal Society of Chemistry.

conformation of the  $\text{Cu}_3\text{S}_3$  hexagons in the  $\text{Cu}(\text{SPhCO}_2\text{Me})$  analogue with the ester functions is half-chair.<sup>[14]</sup>

To date, Cu(SPhCO<sub>2</sub>H), CuHT, and Cu(SPhCO<sub>2</sub>Me) are the only reported three refined structural models of Cubased OMCs that display a layered structure. In these examples, the copper atoms coordinate S atoms from the ligands to form a honeycomb-like Cu<sub>3</sub>S<sub>3</sub> hexatomic ring, and the thiolate moieties stack above and below the layers. For Au(SPhR) (R=CO<sub>2</sub>H<sup>[20]</sup> and CO<sub>2</sub>Me<sup>[13]</sup>), the inorganic layers are quite different from the honeycomb-like Cu<sub>3</sub>S<sub>3</sub> structure, which is constructed by –S–Au–S–Au– chains linked through aurophilic interactions.

Owing to the high reactivity between thiol and gold precursors, the products usually precipitate with poor crystallinity and are usually described as cyclic motifs and polymers. [21] The structures of these products are usually helical or lamellar. Research on the crystal structures of Aubased OMCs is scarce. The first structure elucidation of an Au-based OMC, Au(SPhCO<sub>2</sub>Me), was reported in 2016.<sup>[13]</sup> This compound was obtained by refluxing HAuCl<sub>4</sub> and an excess amount of para-mercaptobenzoic acid in MeOH solution. The full conversion of the carboxyls into methyl esters in Au(SPhCO<sub>2</sub>Me) was confirmed by the conversion of p-SPhCO<sub>2</sub>H to esterified disulfide (p-SPhCO<sub>2</sub>Me)<sub>2</sub>. The structure was resolved from powder X-ray diffraction (PXRD) data (Figure 5). Each Au atom is connected by μ<sub>2</sub>bridged S atoms to form a zigzag chain. The Au-S-Au and S-Au-S angles are 97.09(2) and 177.47(4)°, respectively. Owing to the aurophilic interactions between Au-S chains, a planar network of AuS layers is formed. The distance between two Au atoms is 3.199(5) Å, which is less than the sum of the van der Waals radii. The angle between Au atoms is  $168.34(1)^{\circ}$ , which is a slightly off linear. The  $-\text{PhCO}_2\text{Me}$  organic groups cover both sides of the AuS layers.

Another structure of an Au-based OMC, Au-(SPhCO<sub>2</sub>H), was also resolved by PXRD as shown in Figure 6.<sup>[20]</sup> Different from the AuS line in Au(SPhCO<sub>2</sub>Me), the AuS line here is helically arranged, with Au<sup>I</sup> atoms bridged by thiolate ligands on either side. The S-Au-S angles are uncommon in this AuS line. Each helical AuS chain connects with one another through zigzag aurophilic interactions to form a lamellar structure. Carboxylic acids cover the upper and lower sides of the AgS layer. Hydrogen bonds are formed between two adjacent layers.

As mentioned above, silver alkanethiolates were synthesized in 1991; due to technical limitations at that time, only powder XRD and spectroscopic methods were used to analyze the structure. [22] The structure of Ag(SPh) was first investigated by Mazzoni et al. in 2016 using first-principles calculations, [23] and a layered structure was established. The first definite structure of a silver-based OMC is that of NH<sub>4</sub>Ag(SPhCO<sub>2</sub>) reported by Xu et al.<sup>[17]</sup> Due to the small size of the microplates, this structure could not be resolved by using single-crystal structure analysis. The structure was resolved by 3D ED. This compound crystalizes in the monoclinic space group C2/c. As a substructural unit, [AgS<sub>4</sub>] tetrahedrons are formed by one Ag atom connected to four S atoms from para-mercaptobenzoic acid (Figure 7). A onedimensional (1D) polyhedron chain is formed by the [AgS<sub>4</sub>] tetrahedrons through edge-sharing along the c-axis. Adjacent 1D polyhedron chains further cross-linked laterally through the Ag atoms to form a two-dimensional AgS layer. para-Mercaptobenzoic acid molecules are located on the upper and lower sides of the AgS layer as found in other OMCs. The carboxyl from para-mercaptobenzoic acid is deprotonated, which was balanced by free ammonium (NH<sub>4</sub><sup>+</sup>) cations through electrostatic interactions. The spacing between the two layers is 1.89 nm, which corresponds to the atomic arrangement in the filtered (high-resolution transmission electron microscope) HRTEM image. The simulated XRD data are in good agreement with the experimental data.

The structure of AgSPh (Figure 8) was resolved with the latest technological development in analysis, smSFX;<sup>[18]</sup> it

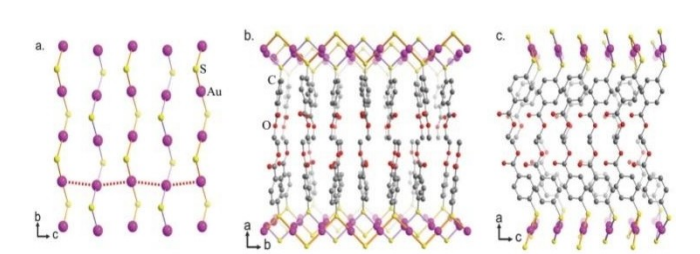


**Figure 5.** Structure of Au(SPhCO<sub>2</sub>Me). a) View of the inorganic layer in Au(SPhCO<sub>2</sub>Me); the gold—thiolate chain is connected through aurophilic bonds. b, c) 3D structure of Au(SPhCO<sub>2</sub>Me) viewed along the c (b) and b (c) direction. Copyright 2016 Royal Society of Chemistry.

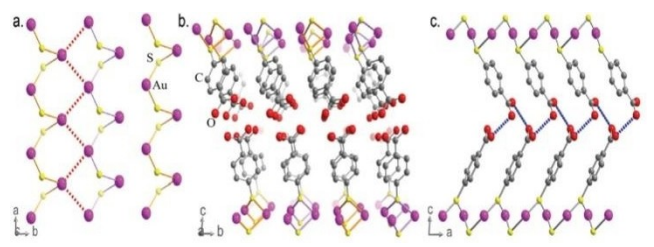


**Figure 6.** Structure of Au(SPhCO<sub>2</sub>H). a) The inorganic layer in Au-(SPhCO<sub>2</sub>H), aurophilic interactions are indicated by dotted lines . 3D structure of Au(SPhCO<sub>2</sub>Me) viewed along the a (b) and b (c) directions. [20] Copyright 2017 Royal Society of Chemistry.





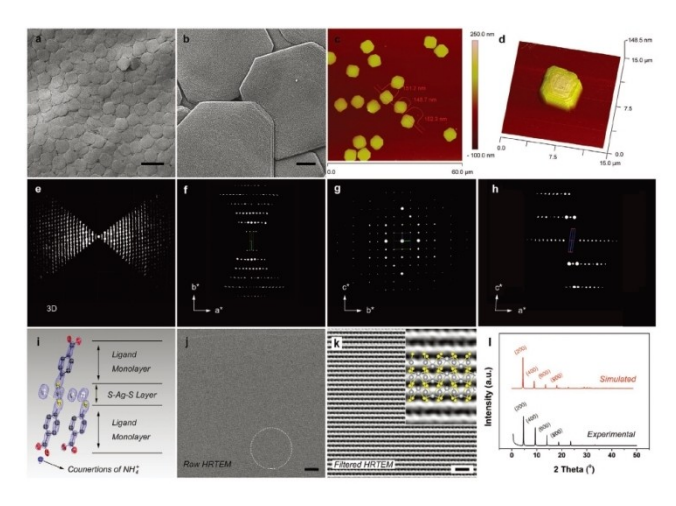


Figure 7. Morphology and structure of  $NH_4Ag(SPhCO_2)$ . a, b) Scanning electron microscopy (SEM) images of the products. c, d) Atomic force microscopy (AFM) images of the microplates. e) 3D reciprocal lattice of the microplates. f–h) 2D slices along  $c^*$ ,  $a^*$ , and  $b^*$  from the 3D reciprocal lattice, i) Structure of  $NH_4Ag(SPhCO_2)$ . j), k) Original and filtered high-resolution transmission electron microscopy (TEM) images viewed along [100]. Inset is the AgS structural model in  $NH_4Ag(SPhCO_2)$ . l) Powder X-ray diffraction (XRD) patterns of the products. [17] Copyright 2021 Wiley-VCH.

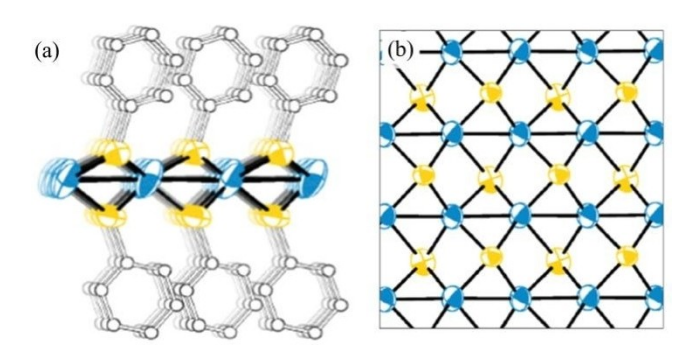


Figure 8. Crystal structure of AgSPh. a) Side view of AgSPh. b) The AgS layer. [18] Copyright 2020 Springer Nature.

shows a lamellar structure similar to that of  $NH_4Ag$ -( $SPhCO_2$ ). The only difference is that the Ag atoms form a linear Ag-Ag chain, which alternately stacks in the AgS layer. This structure further affects the properties of the material.

#### 2.2. Two-Dimensional OMCs Based on MSex Layers

The structure of MSe<sub>x</sub>-based OMCs is rarely reported in the literature. Silver benzeneselenolate (AgSePh) is the only case that has above two-dimensional layered structure. It is a direct gap semiconductor and the exciton binding energy is large;<sup>[4,24]</sup> its optical properties are similar to those of transition metal dichalcogenide monolayers such as MoS<sub>2</sub>.<sup>[4,25]</sup> AgSePh was first prepared by Corrigan and coworkers through the reaction of AgCl and PPh<sub>3</sub> with either PhSe<sup>-</sup> or PhSeS<sup>-</sup>.<sup>[8]</sup> The crystal structure reported by

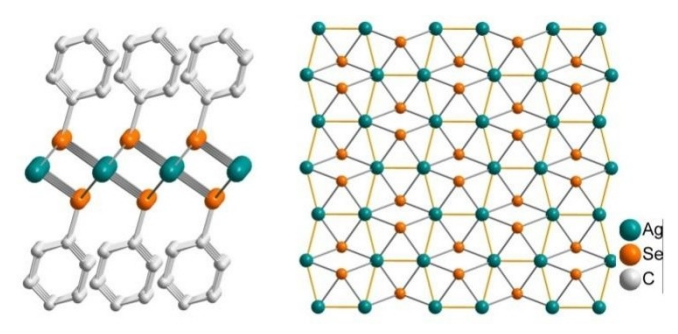


Figure 9. The side view of AgSePh and the top view of the AgSe layer. [18] Copyright 2020 Springer Nature.

Corrigan and co-workers (Figure 9) was obtained in the monoclinic space group of C2/c with two independent Ag atoms, which thereby adopt an elongated hexagonal lattice that forms a network of distorted  $Ag_6$  hexagons through Ag. Ag interactions. Each Ag atom coordinates with four S atoms to form a distorted tetrahedral coordination. The benzene rings connected to the AgSe layer through C–S covalent bonds lying above and below the Ag plane to form a sandwich structure as a supramolecular multi-quantum-well structure. The adjacent benzene layers are bonded together by van der Waals forces, and the thickness of one layer is 1.4 nm.

Single crystals of AgSePh prepared by biphasic synthesis are about 3 µm in size. [25a] Tisdale et al. found that the size and quality of AgSePh crystals can be improved by adding amines in a solution-phase growth process. [26] The average size of AgSePh microcrystals can be increased from  ${<}5\,\mu m$ to >1 mm by inducing the formation of silver-amine complexes during the crystal growth. When the reaction conditions were optimized, single crystals with a size of at least  $\approx 200 \, \mu \text{m} \times \approx 200 \, \mu \text{m} \times \approx 20 \, \mu \text{m}$  could be obtained, and the quality of such product was sufficient for structural refinement by SC-XRD. An AgSePh crystal obtained by this method is best refined as the monoclinic space group  $P2_1/c$ . This assignment differs from the C2/c space group reported by Corrigan et al., which could be due to the higher crystal quality and reduced contact twinning or the existence different synthesis polymorphs formed under conditions.<sup>[26]</sup> The amine-assisted crystal growth method can also be used for other OMCs, such as AgSePhMe (SePhMe=4-methylphenylselenolate). As shown in Figure 10, the single crystal of silver 4-methylphenylselenolate, crystallized in the monoclinic space group  $P2_1/c$  with a monolayer thickness of 1.7 nm, shows a structure similar to that of AgSePh.

#### 2.3. Two-Dimensional OMCs Based on MTe<sub>x</sub> Layers

Obtaining Te-based OMCs is much harder. Thanks to the smSFX technique, tethrene AgTePh is the only reported Te-based OMC.<sup>[18]</sup> As shown in Figure 11, the structure closely resembles AgSePh, with only small distortions to accommodate the longer Ag—Te bonds.





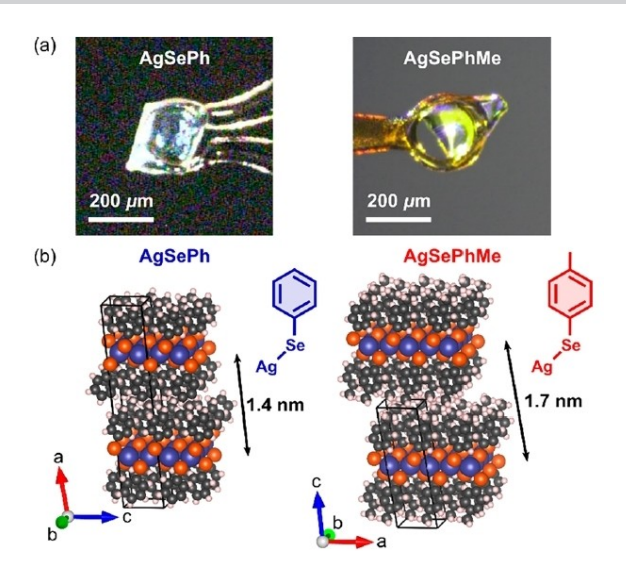
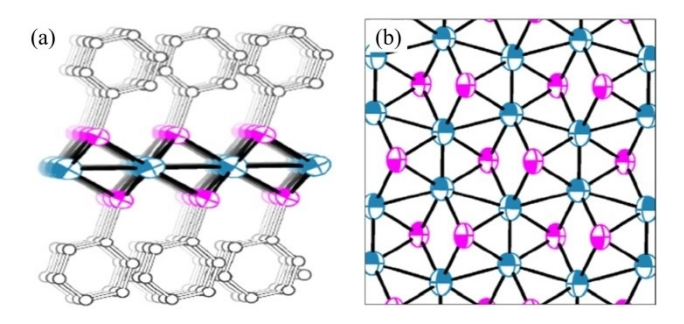


Figure 10. Single crystal images (a) and crystal structures (b) of AgSePh and AgSePhMe. [26] Copyright 2021 American Chemical Society.



**Figure 11.** Crystal structure of AgTePh from smSFX. $^{[18]}$  Copyright 2022 Springer Nature.

# 2.4. Two-Dimensional OMCs Based on Other Element-Doped MS, Layers

In addition to pure MS layers, other coordination bonds can make up the inorganic layer to form a similar superlattice structure. Notably, in this OMC system, separate two-dimensional layers can be formed between the metal and the chalcogen atoms, even when the doped elements are removed. N-donor groups are the most commonly used modifications to  $MS_x$  layer (Figure 12).  $Ag(C_5H_4NS)$  ( $C_5H_4NSH=2$ -mercaptopyridine) with a graphite-like array

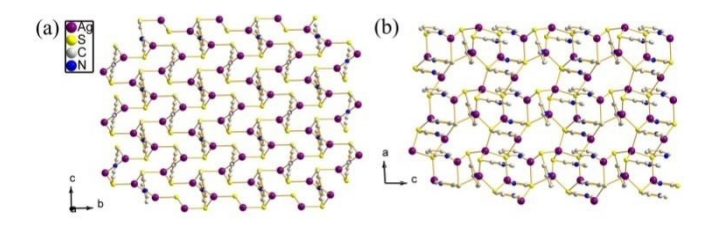


**Figure 12.** Top view of crystal structures of  $Ag(C_5H_4NS)$  (a) and  $Ag_5(C_5H_4NS)_4(C_5H_5NS)BF_4$  (b).

of Ag ions was reported by Hong and Cao et al.<sup>[7]</sup> Each Ag atom is coordinated by one N atom and two S atoms from three PyS<sup>-</sup> ligands in a distorted trigonal-planar fashion. Each PyS<sup>-</sup> ligand here acts as a  $\mu_3$  bridge to link two Ag atoms through the S atom, and ligates another Ag atom through the N atom. The Ag atoms, arranged to form a graphite-like hexagonal Ag<sub>6</sub> motif, are nearly coplanar. This Ag<sub>6</sub> network is connected by S and N atoms to form a two-dimensional lamella structure, whereas the pyridyl groups from the PyS ligands protrude into the layer, which is similar to the OMC structure in OMCs. The interlayer distance is 17.17 Å, which is a little longer than that between AgS layers.

The reaction of Ag and PySH is highly dependent on the solvent.  $Ag_5(C_5H_4NS)_4(C_5H_5NS)BF_4$  with two-dimensional motif can be obtained in  $CH_3CN$  and  $H_2O$  solvent at room temperature. In  $Ag_5(C_5H_4NS)_4(C_5H_5NS)BF_4$ , in contrast to  $Ag(C_5H_4NS)$ , pyridine-2-thiolate has two forms: pyridine-2-thiolate and 1*H*-pyridine-2-thiolate. As a result, the coordination modes of the ligands and Ag atoms are different from that in  $Ag(C_5H_4NS)$ . Unlike the graphite-like array of the hexagonal  $Ag_6$  motif in  $Ag(C_3H_4NS)$ , Ag atoms are irregular in  $Ag_5(C_3H_4NS)_4(C_5H_5NS)BF_4$ . Furthermore, because of the protonation of pyridine,  $BF_4^-$  ions are embedded in the interlayer region.

In a modification of the  $C_5H_4NS$  ligand, the position para to S has a carboxyl substituent. Lu et al. reported highly conductive  $[Cu_2(6\text{-Hmna})(6\text{-mn})]\cdot NH_4$  (6-Hmna=6-mercaptonicotinic acid, 6-mn=6-mercaptonicotinate). Different from CuHT, where the Cu centers adopt a  $CuS_4$  tetrahedral geometry, here one S is replaced by N from the 6-Hmna ligand to form a  $[CuS_3N]$  unit. The Cu and S atoms are arranged in a honeycomb-like structure in the ab plane (Figure 13). These  $(-Cu-S-)_n$  sheets are arranged in a parallel manner along the c axis and are further connected by 6-Hmna and 6-mn ligands. The distance between two

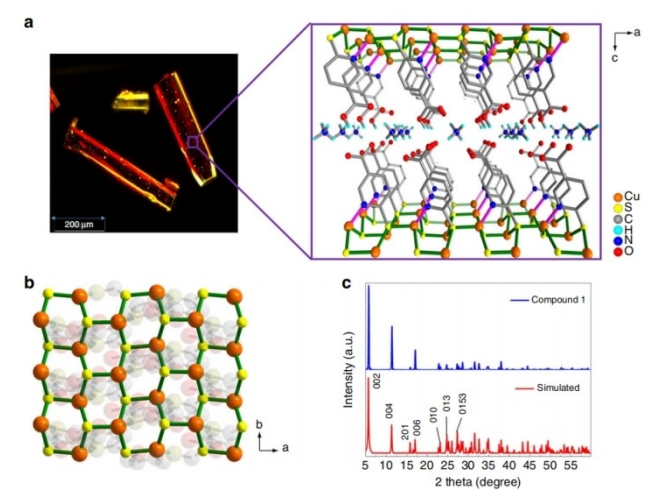


**Figure 13.** Structure of [Cu<sub>2</sub>(6-Hmna) (6-mn)]·NH<sub>4</sub>. a) Dark-field optical image and enlarged structure viewed along the c axis (Cu, orange; O, red; C, light gray; N, blue; S, yellow; H, cyan). b) (-Cu-S-)<sub>n</sub> sheets in the layer. c) As-synthesized and simulated PXRD patterns. <sup>[16]</sup> Copyright 2019 Springer Nature.





layers is 14.4 Å which is similar to that in CuHT. Considering the deprotonation of the carboxylic acid group on the ligand, the whole inorganic layer has a negative charge. As a result, ammonium ions  $(\mathrm{NH_4}^+)$  are incorporated into the framework as counter ions.

In addition to the pyridine-thiolate ligands, the ligands resulting from amino substitutions on the benzene ring can form similar layered structures. Single crystals of Cu(abt) (abt=2-aminobenzenethiolate) can be formed by the reaction of 2-aminobenzenethiol and CuI in DMF. [10] For the coordination of N and S atoms to Cu atom (each Cu atom is coordinated in a pseudo-tetrahedral fashion by one N and three  $\mu_3$ -bridging S atoms), the layer in Cu(abt) closely resembles black phosphorus (Figure 14), which is composed of a zigzag (Cu–S) double-layered network.

Besides benzene-based ligands, heterocyclic rings can also connect to the S to form layered OMCs. Ag<sub>2</sub>-(H<sub>2</sub>trzS)<sub>2</sub>Cl<sub>2</sub> (H<sub>2</sub>trzS = 1H-1,2,4,-triazole-3-thiol), which was reported by An et al., was synthesized using solvothermal methods. Ag<sub>2</sub>(H<sub>2</sub>trzS)<sub>2</sub>Cl<sub>2</sub> shows a two-dimensional layer structure constructed by an inorganic graphite-like [AgS]<sub>n</sub> layer, which is similar to the CuS layer in [Cu<sub>2</sub>(6-Hmna)(6-mn)]·NH<sub>4</sub>. The five-membered N-heterocycles and Cl– ions cover the [AgS]<sub>n</sub> layer above and below (Figure 15).

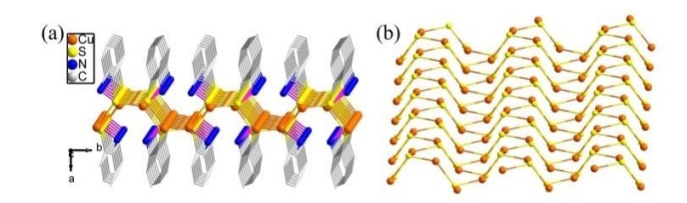
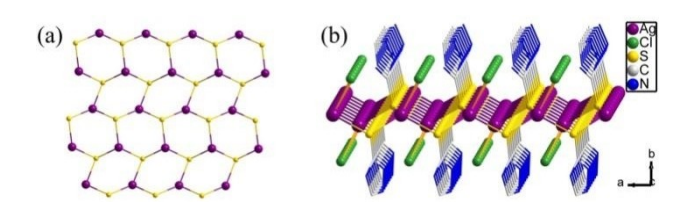


Figure 14. Side view of Cu(abt) (a) and zigzag (Cu-S) double-layered network in Cu(abt) (b).



**Figure 15.** a) Graphite-like  $[AgS]_n$  layer in  $Ag_2(H_2trzS)_2Cl_2$ . b) Side view of the layer. [11] Copyright 2013 Elsevier.

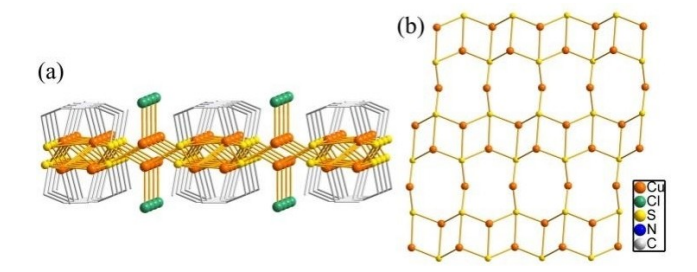


Figure 16. Crystal structure of  $Cu_3Cl(SR)_2$ . a) Side view. b) The CuS layer.

In the case of  $\text{Cu}_3\text{Cl}(\text{SR})_2$  ( $\text{R}=\text{CH}_2\text{CH}_2\text{NH}_2$ ), [12] the Cu shows a trigonal-planar structure, while each S atom bridges four Cu atoms. The CuS layer is sandwiched between halogen and alkyl chains to form a sandwich structure (Figure 16).

### 3. Synthesis Strategies for Nanosheets and OMCs

#### 3.1. Synthesis of OMC Nanosheets

As this material system has not been studied for long, most studies focus on the acquisition of bulk materials and a few reports concern the morphology of the materials. Multilayer nanosheets, as an intermediate state between bulk material and 2D material, with thickness ranging from dozens to hundreds of nanometers are also worth mentioning; they can obtained by the solvothermal/solution method. Polycrystalline nanosheets of CuHT were obtained by refluxing an ethanolic suspension of Cu<sub>2</sub>O and 4-mercaptophenol. Single crystals with thin pellets of Cu(SPhCO<sub>2</sub>Me) can be formed by a redox reaction between Cu(NO<sub>3</sub>)<sub>2</sub> and *p*-HSPhCO<sub>2</sub>Me under solvothermal conditions. Uniform octagonal plates of NH<sub>4</sub>Ag(SPhCO<sub>2</sub>) with a lateral dimension of 5.5 µm and a thickness of 150 nm are formed by bottom-up synthesis.

Beside one-pot procedures, the interface-mediated synthesis method is mainly used to obtain films composed of nanosheets. The interface-mediated synthesis method is a technique in which the products grow at the air/liquid, liquid/liquid, or solid/gas interface. As a promising route, the interface approach is very important for the assembly of extended nanosheets. Allen et al. found that a film of Ag alkanethiol self-assembled monolayers can be grown on planar Ag thin films, whereas two dissimilar products will appear on Ag islands.<sup>[27]</sup> For AgSePh, layered crystals can be grown at the immiscible water-toluene interface, [25a,b] but in a solvent-free reaction between gas-phase diphenyl diselenide (DPSe) and silver metal, the products appears to be corrosion-like 200 nm-thick films (Figure 17).[4] A film made up of AgSePh nanocrystals can also be obtained on the gas/ solid interface of benzeneselenol and AgO. [28] Although a relatively uniform membrane can be obtained from this interface-mediated method, the thickness of this material needs to be further optimized to obtain thinner material with few layers or even a single layer.

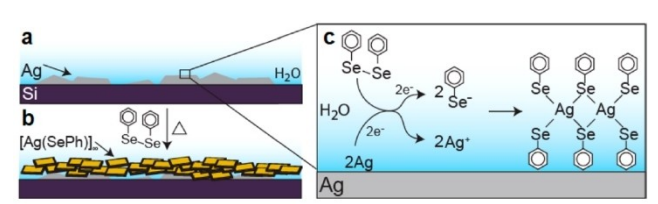


Figure 17. Schematic overview of the reaction between Ag and DPSe. [4] Copyright 2018 American Chemical Society.





#### 3.2. Top-Down Method for OMC Synthesis

Owing to the weak interactions between layers (such as van der Waals forces, coulomb force, and hydrogen bonding), the top-down method is a powerful approach to break down bulk OMCs into nanosheets with a few layers. Among the numerous methods, sonication-assisted liquid exfoliation is a very important and widely used approach.<sup>[29]</sup> Under exfoliation conditions that were optimized in terms of the type of solvent, the power and time for sonication, as well as the rate and period for centrifugation, few-layer CuHT, Cu-(SPhCO<sub>2</sub>H) (HSPhCO<sub>2</sub>H = para-mercaptobenzoic acid), Ag- $(SPhCO_2H),\ Au(SPhCO_2H),\ Ag(SPhNH_2)\ (HSPhNH_2\!=\!4\!-\!$ aminobenzenethiol), Ag(HT), Ag(SPhOCH<sub>3</sub>)  $(HSPhOCH_3 = 4-methoxybenzenethiol),$ and Ag(SPhF)

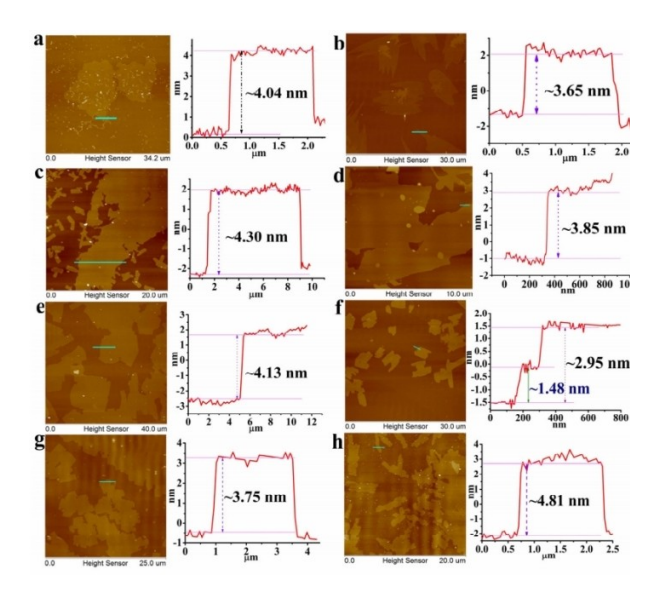


Figure 18. AFM images of a) CuHT, b) Cu(SPhCO<sub>2</sub>H), c) Ag(SPhNH<sub>2</sub>), d) AgHT, e) Ag(SPhOMe), f) Ag(SPhF), g) Ag(SPhCO<sub>2</sub>H) and h) Au-(SPhCO<sub>2</sub>H) on SiO<sub>2</sub>/Si substrates. [3] Copyright 2020 Springer Nature.

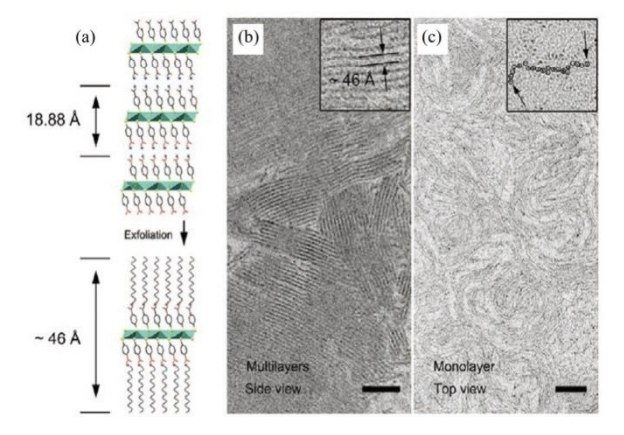


Figure 19. a) Structure illustration of NH₄Ag(SPhCO₂) before and after exfoliation with cetyltrimethylammonium bromide (CTAB). The corresponding TEM images (insert shows an enlarged section of the products) collected after 1 h (b) and 3 h (c). [17] Copyright 2021 Wiley-MCM.

(HSPhF=4-fluorobenzenethiol) can be prepared by a liquid exfoliation method (Figure 18).<sup>[3]</sup>

Apart from the solvent, surfactants (such as cetyltrimethylammonium bromide (CTAB)) can also influence the exfoliation efficiency. When large CTA<sup>+</sup> cations are incorporated into NH<sub>4</sub>Ag(SPhCO<sub>2</sub>), the small NH<sub>4</sub><sup>+</sup> ions are replaced by CTA<sup>+</sup>, and a multilayer stacking structure with an interlayer distance of 46 Å can be obtained following ultrasonic treatment for 1 h. When the ultrasound time is extended to 3 hours, infinite ultrathin 2D AgS networks protected by a *para*-mercaptobenzoic acid bilayer can be obtained. For the protection of CTA<sup>+</sup>, these infinite ultrathin sheets are stable in solvent, such as water and/or ethanol (Figure 19).<sup>[17]</sup>

Besides CTA<sup>+</sup>, sodium citrate (CA–Na) is also found to be a good choice as an exfoliation agent for the exfoliation of Au(MPA) (MPA=S(CH<sub>2</sub>)<sub>2</sub>COOH) nanosheets. [30] CA–Na acts as not only a pH regulator but also as a surfactant to enhance the dispersibility of the nanosheets. By using different amounts of CA–Na, the thicknesses of the Au(MPA) nanosheets can be adjusted from dozens of nanometers to several nanometers.

#### 3.3. Bottom-Up Self-Assembly Method for OMC Synthesis

The bottom-up one-step synthesis is the most expected and the most efficient way to prepare OMCs. To use this method, it is also important to study the dynamic growth process. The dynamic assembly of Au(MPA) lamella can be monitored by molecular-level time-resolved characterization methods. First, a rod thread rigid-flexible "block copolymer" conformation is formed through the randomly distributed intrachain aurophilic interactions (AIs) (Figure 20a). Long string structures are further formed by interchain AIs (or together with hydrogen bonds) (Figure 20b). To strengthen the AIs, the rod conformations become longer and the string structures tend to turn or even break at the flexible parts to form coil structures (Figure 20c). Larger extended structures are generated by

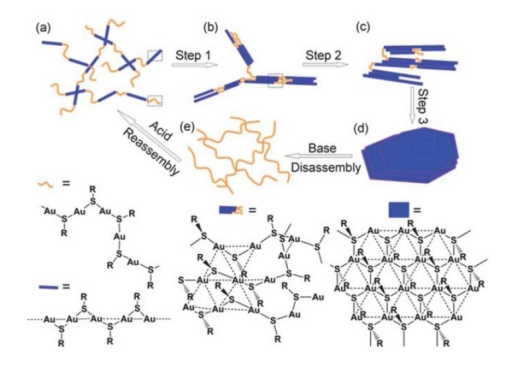


**Figure 20.** Scheme of the assembly progress of Au(MPA). a) Rod-thread "block copolymer" conformation of Au(MPA); b) String structures; c) Coil structures resulting from alignment of the string structures; d) Lamellar structures by further coordination of S to Au; e) AuMPA chains; R is  $-CH_2CH_2COOH$  (or Na). [31] Copyright 2018 Royal Society of Chemistry.





further extending and stacking of the coil structures (Figure 20d). Addition of base to the above products repulses the lamellar nanosheets to flexible chains again (Figure 20e), whereas the introduction of acid into the solution will induce reassembly again. The study of this dynamic process provides many bases for the growth of two-dimensional materials.

The hydro/solvothermal synthesis method is a classical and widely used strategy to synthesize bulk and 2D materials. Lin et al. synthesized CuCl<sub>x</sub>(MBA)<sub>y</sub> nanosheets with a thickness of 8 nm.<sup>[32]</sup> During the synthesis process, the use of different concentrations, temperatures, and solvents led to distinct molecular packing modes, resulting in products with different structures and phenomena. The thickness of spindle-shaped nanosheets Au(MPA) is 3 nm in water solution, whereas in ethylene glycol, there are two types of products: triangular flakes with a thickness of 3 nm and an irregular aggregate with a thickness of tens of nanometers (Figure 21).<sup>[33]</sup>

Li et al. found that the size and thickness of the products highly depends on the pH value.<sup>[34]</sup> Changing the [COO<sup>-</sup>]/[COOH] ratio in Au(MPA) can gradually influence the pH value of the solution; increasing the pH of the solution will prohibit the further growth of the smaller species. Microscopic precipitates of Au(MPA) are generated immediately after mixing MPA with HAuCl<sub>4</sub> without CA–Na. The size of the Au(MPA) can be continuously reduced from bulk to nanoscale and the assembly time can be lengthened to minutes by tuning the concentration of CA–Na.<sup>[31]</sup>

The internal structure and geometrical morphologies of the products can also be adjusted by introduction of a coligand. A series of thiol ligands (thioglycolic acid (TGA), thioglycerol (TGO), cysteine (Cys), penicillamine (Pen) and cysteine-glycine dipeptide (CG)), which serve as a second ligand with different functional groups and sizes, were screened for the synthesis of Au(MPA). The results shows that ligands (TGO and Cys) with similar sizes to MPA can co-assemble with MPA in a large percentage. The thickness

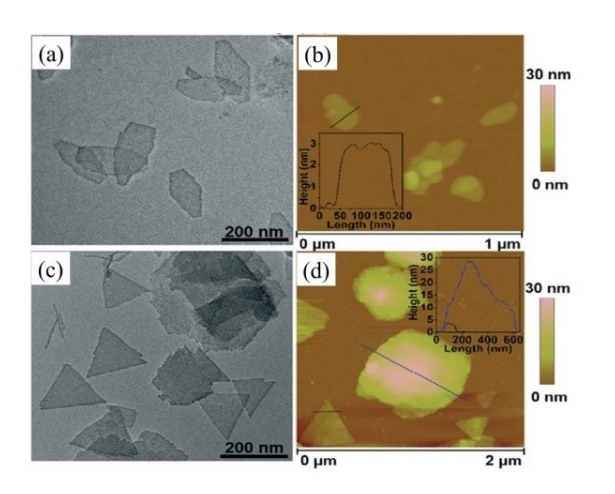


Figure 21. a, c) TEM images and b, d) AFM images of Au(MPA) in water (a, c) and Au(MPA) in EG (b,d). Inset: Height analyses of typical samples. [33] Copyright 2018 Royal Society of Chemistry.

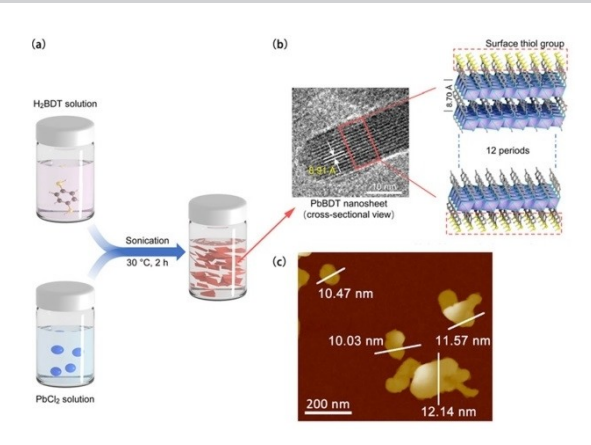


Figure 23. a) Fabrication of PbBDT nanosheets. b) HRTEM image and crystal structure. c) AFM image. [36] Copyright 2021 Wiley-VCH.

of the Au-MPA-co-Cys(TGO) nanosheets is 3–5 nm. The introduction of the second ligand has little effect on the thickness of the nanosheets, but it affects the morphology (Figure 22).

In the above method, the few-layered nanosheet is exfoliated from the OMC precursors. Another way to obtain such ultra-thin nanosheets fully covered by functional groups is synthesis directly from organic–inorganic hybrid superlattices under controlled reaction conditions. Nanosheets of PbBDT (BDT=1,4-benzenedithiolate) with a thickness of  $\approx 11$  nm can be obtained directly by the solution method (Figure 23). Notably, the surface of the nanosheet is orderly covered by SH functional groups, which is very similar to OMCs. Although the thickness of this material is not limited to a few atomic layers, it provides a new strategy for synthesizing OMCs. [36]

#### 3.4. Characterization of OMCs

For large-sized crystals, the structure can be determined by single-crystal X-ray diffraction, but for nano- or submicronsized samples, 3D ED or smSFX is needed. With the

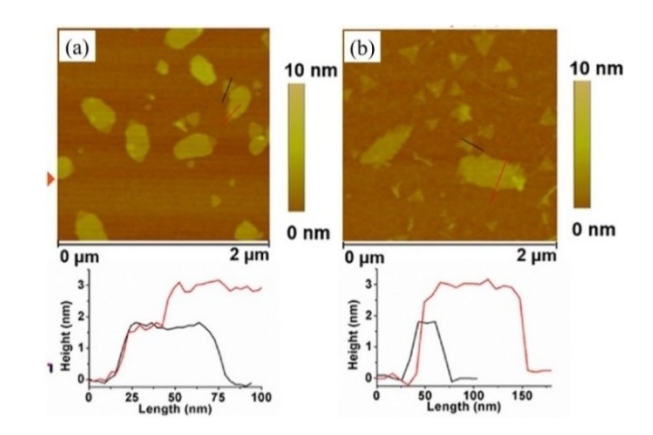


Figure 22. AFM image and the height analyses of Au-7MPA-co-Cys (a) and Au(MPA) (b) nanosheets. [35] Copyright 2017 Wiley-VCH.





development of nanotechnology, many useful and advanced characterization techniques have been developed, such as optical microscopy, atomic force microscopy, powder X-ray diffraction scanning probe microscopy, scanning electron microscopy, transmission electron microscopy/scanning transmission electron microscopy, X-ray absorption fine structure spectroscopy, X-ray photoelectron spectroscopy, and Raman spectroscopy. [1a] The composition, size, thickness, crystallinity, crystal phase, and defects can be confirmed through these techniques. As a two-dimensional material, the above techniques also apply to OMCs. The functional groups on OMCs can be characterized by infrared and Raman spectroscopy, elemental analysis, and mass spectrometry.

### 4. Applications of Nanosheets and OMCs

The organic modifiers on the surface of the inorganic metal chalcogenides act as a chemical gating, which is similar to the electrical gating in FETs. The stronger electron-donating ability results in a stronger electric dipole and thus more injected holes and a higher conductivity in p-type OMCs.[3] Additionally, through the modification of electron donating strength of these organic functional motifs, the surface energetics and electron transfer resistance of the metal chalcogenides can be regulated, which further affects the activity of OMCs. Considering their unique structural characteristics, high degree of structural designability for coordinate chemistry assembly, high number of active functional sites on the surface of the two-dimensional layer, good electrical conductivity of the inorganic layers, and ease in exfoliation into few-layer materials, OMCs are becoming excellent candidates for functional components in photoelectrical and electrochemical domains, such as in chemiresistive gas sensors and in energy conversion.

### 4.1. Photoelectric Detectors

Hybrid quantum wells are constructed by the alternate stacking of inorganic and insulating organic layers, where the carriers are confined in the inorganic layer. This unique structure makes them promising candidates for optoelectronic devices. OMCs, possessing an organic-inorganic alternating quantum-well superlattice structure, are potential photoelectric detection materials. The charge carriers of AgSePh have been proven to be confined on the AgS layer by optical spectroscopy.<sup>[37]</sup> The optoelectrical response of a AgSePh single crystal was first investigated by Xu et al. (Figure 24).<sup>[38]</sup> The on/off ratio increases by nearly two orders of magnitude upon irradiation with periodic light pulses with a response time  $(\tau_{rise})$  and a decay time  $(\tau_{decay})$  of 0.94 and 0.045 s, respectively. The  $R_{\lambda}$  and detectivity  $(D^*)$ are 0.119 A W<sup>-1</sup> and 1.29×10<sup>11</sup> Jones, respectively, under a bias of 2 V.

Maserati et al. first investigated the electrical properties of the air-stable AgSePh nanocrystal (NC) film (Figure 25).<sup>[28b]</sup> The devices showed a wavelength-dependent

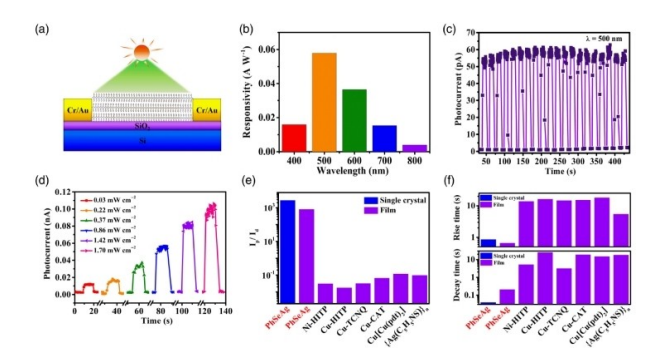


Figure 24. Photodetection measurements of AgSePh. a) Schematic illustration of a single-crystal-based photodetector. b) Responsivities at different wavelengths. c) Photoresponse of AgSePh under periodic illumination. d) Photoresponse of AgSePh under different light intensities. e) Comparison of the response with that of other conductive coordination polymers. f) Rise time and decay times with different coordination polymers. [38] Copyright 2020 Chinese Chemical Society.

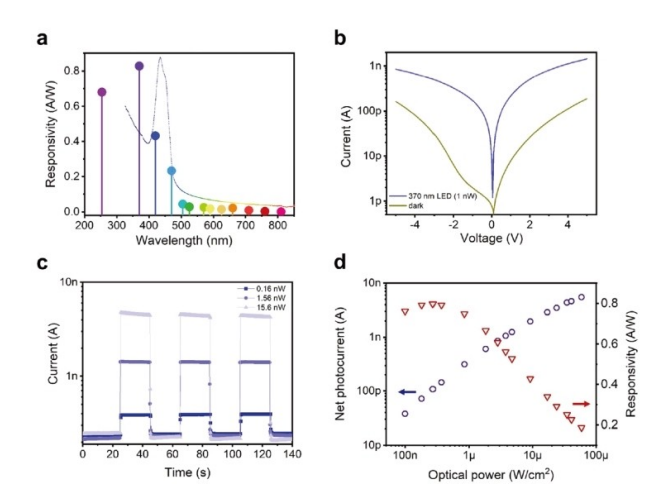


Figure 25. UV photosensor characteristics of AgSePh NC film. a) Norrmalized photocurrent response (constant irradiance 300 nW cm<sup>-2</sup>) and absorption profile of AgSePh NC film. b) I–V curve characteristics in the dark and under monochromatic (LED) illumination at 370 nm. c) Photocurrent response of AgSePh NC film under different illumination powers, at 370 nm and 5 V applied bias. d) The net photocurrent and responsivity under incident power density.<sup>[286]</sup> Copyright 2021 Royal Society of Chemistry.

photocurrent response; interestingly, the highest photoresponse is in the UV range other than the maximum light absorption. This phenomenon may correspond to the excitonic resonances. The maximum responsivity is  $\approx\!0.8~\text{A}\,\text{W}^{-1}$  at 370 nm. The cut-off frequency of lateral device is approximately 400 Hz, and the on/off ratio is approaching 1000 under broadband illumination.

#### 4.2. Photoluminescence

Considering the metal-centered transition and ligand-tometal electron transfer (LMCT), OMCs are a good emitters, and exhibit low-energy green or red emission. Cu<sub>3</sub>Cl(SR)<sub>2</sub>





shows red light emission under excitation at 360 nm.<sup>[12]</sup> AuSR exhibits red light emission centered at 620 nm under excitation by UV irradiation.<sup>[39]</sup> Demessence et al. reported an ultra-bright photoluminescence from Au(SPhCO<sub>2</sub>Me) powder.<sup>[13]</sup> The color of the emission can be manipulated by doping with other metals. The emission of Ag(SR) can be changed from green to red by Cu doping (Figure 26).<sup>[40]</sup>

Another way to change the emission color of the material is to change the excitation wavelength. Ag-(SPhCO<sub>2</sub>H) shows high-energy emission under excitation at 220–340 nm, whereas lower energy emission can be observed under excitation at 360 nm. Ag(SPhCO<sub>2</sub>Me) shows both high-energy emission and low-energy emission (650 nm) when excited at 220–360 nm, and shows low-energy emission at 700 nm under 380 nm excitation. As explained, the emission in the high-energy range comes from the ligand-centered  $\pi$  to  $\pi^*$  transition while emission in the low-energy originates from the LMCT.  $^{[40]}$ 

Different from the luminescence caused by traditional electron transfer, the unique luminescence of OMC comes from its unique multi-quantum-well structure. Benefitting from the unique structure, the inorganic layers represent the extremum of quantum confinement in semiconductors, down to only one monolayer of unit cell. Strong excitonic effects enhance light-matter interaction, allowing the materials to exhibit strong absorption, reflection, emission, and nonlinear optical responses.

The exciton binding energy is higher than 380 meV in layered bulk AgSePh which is confirmed by the combination of transient absorption spectroscopy and ab initio GW plus Bethe-Salpeter equation calculations. Schuck et al. provided experimental evidence of an exciton binding energy of approximately 0.4 eV with exciton radiative rates of  $\approx 20~\mathrm{ps}$  for the ground state exciton of this material. This value is significantly higher than that of conventional bulk semiconductors and comparable with those observed in atomically thin transition metal dichalcogenides and layered two-dimensional perovskites. AgSePh shows robust blue luminescence at 467 nm, with an external quantum efficiency of about 2% at room temperature. The blue emission is not influenced by crystal size, shape, or morphology. The state of the combination of the combination

Schuck et al. also changed the benzene rings in AgSePh to biphenyl and methoxybenzene to elucidate the 2D

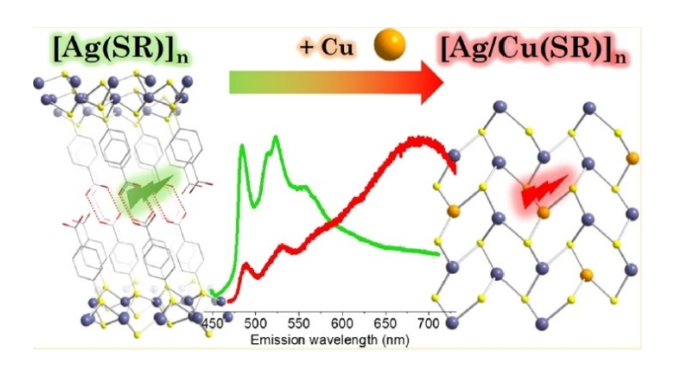


Figure 26. The emission of Ag(SR) and Ag/Cu(SR).  $^{[40]}$  Copyright 2018 American Chemistry Society.

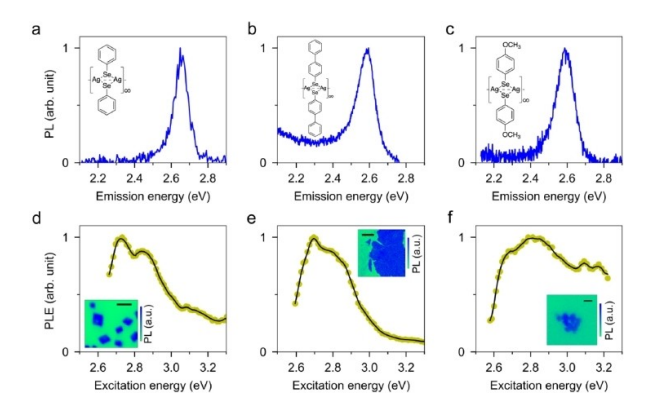


Figure 27. The insensitivity of photoluminescence (PL) and photoluminescence excitation (PLE) of AgSe materials with different organic ligands. a)–c) PL and d)–f) PLE spectra of samples, where the ligands used as the quantum well barrier layers are phenyl, biphenyl, and methoxybenzene, respectively. Insets show the schematic structure in (a–c), and the confocal PL imaging of corresponding samples in (d–f), the scale bars are 2, 20, and 5 μm, respectively. a.u.: arbitrary unit. [24] Copyright 2021 American Chemistry Society.

quantum confined nature of the multi-quantum-well structure. The PL peak energies are quite similar with values of 2.66, 2.58, and 2.59 eV for the mithrene, biphenyl-mithrene, and methoxybenzene-mithrene materials, respectively, which confirms that the band edge states predominantly consist of atomic orbitals within the inorganic AgSe layers and have little contribution from atoms in the organic barrier layer. Photoluminescence excitation spectra with different line shapes for different ligands can be found under photon energy of above  $\approx 3~{\rm eV}$  (Figure 27), indicating the onset of optical transitions in the organic barrier layers. The results demonstrate that the semiconducting AgSe layers are confined by organic ligand barriers in AgSePh.  $^{[24]}$ 

The homologues thiorene (AgSPh), mithrene (AgSePh), and tethrene (AgTePh) have similar layered structures but show different photoluminescent properties. Mithrene is a direct band gap semiconductor that emits blue light with a short photoluminescent lifetime (50 ps). Tethrene possesses an indirect band gap and shows broad emission with a longer lifetime (1 ns). However, thiorene shows no emissive profile in the visible range. These results are attributed to the different inorganic layered structures of these compounds. The excitons in mithrene and tethrene, delocalized in the two-dimensional inorganic layer across the argentophilic network of Ag–Ag bonds, give rise to the visible absorption and emission. The argentophilic interactions of thiorene are marked by linear Ag–Ag chains, which do not support the two-dimensional delocalization of excitons. [18]

#### 4.3. Thermochromic Sensing

Thermochromism is the property of a material to change its color in response to the change in the surrounding temperature. Both Ag(SPhCO<sub>2</sub>H) and Ag(SPhCO<sub>2</sub>Me)<sup>[40]</sup> display thermochromic luminescent response in the solid state (Figure 28), with emission at 700 and 580 nm at 243 K under





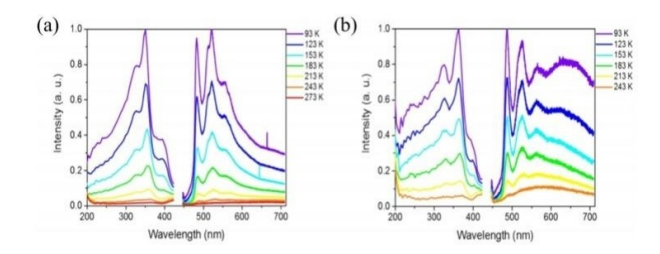


Figure 28. a) Excitation and emission spectra of  $Ag(SPhCO_2H)$  and b)  $Ag(SPhCO_2Me)$ . [40] Copyright 2019 American Chemistry Society.

excitation at 380 and 368 nm, respectively. Excitation (352 nm for  $Ag(SPhCO_2H)$ , and 364 nm for  $Ag(SPhCO_2Me)$  and emissions are shifted to higher energies as the temperature is decreased to 93 K (484/528 nm for  $Ag(SPhCO_2H)$ , 489/526 nm for  $Ag(SPhCO_2Me)$ . The blue-shifted excitation and emission at lower temperature is attributed to the enhanced rigidity of the network that reduces the energy loss from nonradiative decay. The luminescence color of  $Ag(SPhCO_2H)$  shows a thermochromism from yellow to green with decreasing temperature, whereas  $Ag(SPhCO_2Me)$  exhibits a small color variation in the yellow area.

Syntheses of CuCT (CT=4-carboxy-thiophenolate) and CuMCT (MCT=4-methoxycarbonyl-thiophenolate) in micrometer lateral dimensions and sub-micrometer/nanometer thicknesses allows their processing with an organic polymer, such as polyvinylidene difluoride (PVDF), to form thermochromic CuCT@PVDF and CuMCT@PVDF thin films. Both CuCT@PVDF and CuMCT @PVDF show a reversible luminescence color change from pale yellow to green to orange in the case of CuCT@PVDF, and from pale orange to green in the case of CuMCT@PVDF with decreasing temperature (Figure 29). These thermal stimuli-responsive

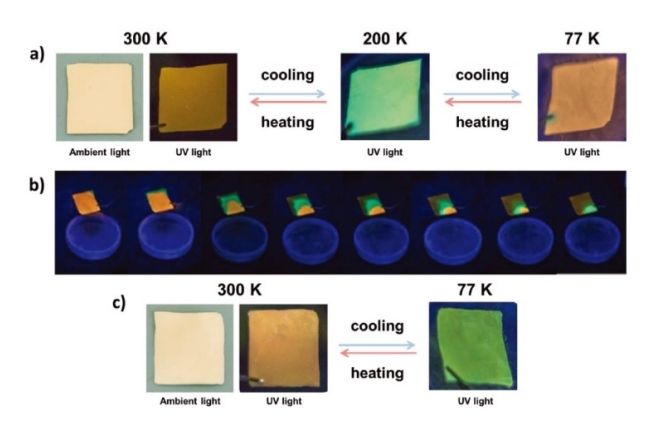


Figure 29. Optical photographs of thermochromic films of CuCT@PVDF and CuMCT@PVDF. a) Solid-state emission of CuCT@PVDF film at different temperatures and excited at 365 nm. b) Sequential luminescence photographs of CuCT@PVDF thin films from 77 K to room temperature under UV lamp excitation (365 nm). c) Solid-state emission of CuMCT@PVDF under ambient light and UV lamp excitation (365 nm) at different temperatures. [41] Copyright 2018 Wiley-VCH.

thin films are freestanding, free of macroscopic defects, and robust under mechanical bending stress, thereby showing potential applications in 2D imaging sensors.<sup>[41]</sup>

#### 4.4. Solar Energy Conversion

Solar energy conversion has been of great interest in developing green and sustainable energy. [42] Thermoelectric materials have attracted much interest due to their potential to convert thermal energy to electrical energy. Pauly et al. calculated the thermoelectric properties of single-layer and bulk copper(I) 4-hydroxythiophenolate (Cu(SC<sub>6</sub>H<sub>4</sub>OH), that is CuHT) and their analogs Cu(SeC<sub>6</sub>H<sub>4</sub>OH) and Cu-(TeC<sub>6</sub>H<sub>4</sub>OH) on the basis of density functional calculations. [43] They found that the performance of these materials is comparable with that of p-type poly(3,4-ethylenedioxythiophene) (PEDOT) and n-type poly[K<sub>x</sub>(Ni-ett)] (ett = ethylenetetrathiolate), which are the reported best organic thermoelectric materials. Wang et al. compounded CuHT with carbon nanotubes (CP-SL). Thermoelectric tests show that CP-SL is a p-type material with a large positive Seebeck coefficient of 307 µV K<sup>-1</sup>, thermal conductivity of 0.31 W m<sup>-1</sup> K<sup>-1</sup>, and electrical conductivity of 0.02 S cm<sup>-1</sup>. [44] Four pairs of p- and n-type thermoelectric modules with alternating CP-SL/CNT and n-type CP-SL/PEI-CNT were made to construct a solar thermoelectric generator (STEG). The temperature differences ( $\Delta T$ ) are 6.5 K, 18.9 K, and 29.4 K, respectively, under the illumination of 1 sun, 3 suns, and 5 suns. The open-circuit voltage and short-circuit current are directly related to the intensity of the illumination light. This STEG device exhibits stable output voltages for long-time use (Figure 30).

### 4.5. Electrocatalysts

High-performance electrocatalysts for electrochemical applications generally require good intrinsic catalytic ability, high porosity, large surface area, multiple atomic active sites, and decent conductivity. [45] Considering the numerous active sites at the center or edges of its inorganic planes and convenient electron transfer through its two-dimensional inorganic layers in OMCs, [Cu<sub>2</sub>(6-mercaptonicotinic acid)(6mercaptonicotinate)]·NH<sub>4</sub>, was electrodeposited onto conductive substrates using poly(3,4-ethylenedioxythiophene) (PEDOT) as the binder (Figure 31), [46] which was further used as the electrocatalyst for the counter electrode in dyesensitized solar cells (DSSCs). Owing to the involvement of Cu-OMCs/PEDOT, the solar-to-electricity conversion efficiency is promoted to 9.45 % at 1 sun and 22.80 % at room light illumination. Compared with the traditional platinum electrode (7.67%), the low-cost Cu-MOF/PEDOT composite electrode has a high possibility of being used for various electrochemical devices and the Internet-of-things applications.





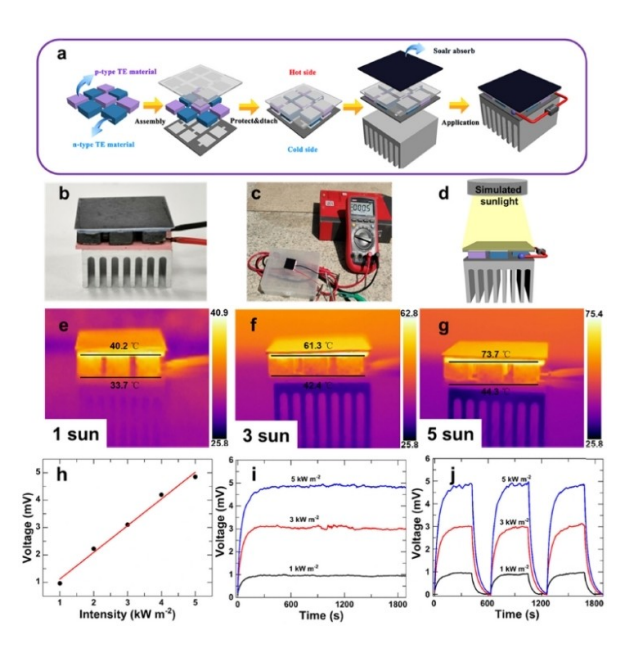


Figure 30. a) Schematic illustration of STEG fabrication. b) Optical image of the STEG. c) Outdoor output voltage of the STEG at 27 °C. d) Schematic diagram of the STEG illuminated by simulating sunlight. e–g) Thermographic image of the STEG taken by an infrared thermal imaging camera under different illumination intensities. h) Open-circuit voltage vs. different illumination intensities. i) Time-dependent output voltages of STEG at different illumination intensities. j) Output response of the STEG under pulse light illumination. [44] Copyright 2021 Elsevier.

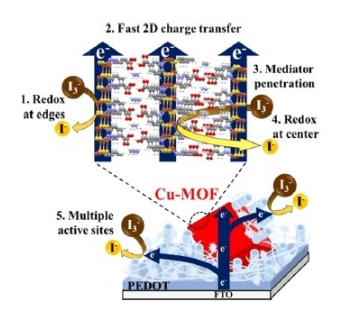


Figure 31. Schematic illustration of the charge-transfer network and the functionalities of the [Cu<sub>2</sub>(6-mercaptonicotinic acid) (6-mercaptonicotinate)]·NH<sub>4</sub>/PEDOT electrode. (46) Copyright 2021 American Chemistry Society.

#### 4.6. Sensors

Considering the large number of functional groups on the surface of the inorganic layer in few-layered nanosheets, these materials can recognize the interference of external gases. Few-layer Ag(SPh–NH<sub>2</sub>) with a thickness of 11 nm is directly synthesized in a solution of AgNO<sub>3</sub> and 4-aminobenzenethiol. As expected, Ag(SPh–NH<sub>2</sub>), with a fully and orderly covering of –NH<sub>2</sub> groups as "receptors", shows the highest sensitivity, excellent selectivity, and reversibility in response to NO<sub>2</sub> among all the reported 2D chemiresistive sensing materials at room temperature. It shows good response–recovery ability over a broad concen-

tration range of  $NO_2$  (0.1–100 ppm) (Figure 32). In situ diffuse reflectance infrared Fourier transform spectroscopy (DRIFTS) measurements were performed to confirm that  $-NH_2$  groups play a critical role in gas sensing. By contrast, Ag(SPh) (HSPh=benzenethiol) without amino functional groups has no response to  $NO_2$ , which further proves that the amino functional groups on the surface of 2D materials play an significant role in the gas sensor.

In addition to gas sensing, 2D OMCs are also used in biological detection. A series of few-layered CuHT, CuM-BA, and AgHBT (HT=4-hydroxythiophenol, MBA=4mercaptobenzoate) 2D OMCs with a thickness of only two to three molecular layers were used as a peroxidase-like catalyst. Through coupling the oxidation of glucose catalyzed by glucose oxidase, the chromogenic reaction catalyzed by CuHBT was further developed into a cascade reaction to quantitatively analyze for glucose (Figure 33). The limit of detection (LOD) toward glucose is approximately 0.172 µM. CuHBT had the lowest detection limit among the reported 2D materials and their composite materials in the one-pot colorimetric detection of glucose. A mechanistic study revealed that the Ph-OH groups on the CuHT surface act as "promoters" and can significantly enhance the performance of the 2D catalyst. [48]

The organic modifiers on the surface of the inorganic metal chalcogenides act as chemical gating, which is similar to the electrical gating in FETs. By finetuning the electron donating strength of the organic modifiers, the surface energetics and electron transfer resistance of the metal chalcogenides can be regulated, which further affects the activity of OMCs.

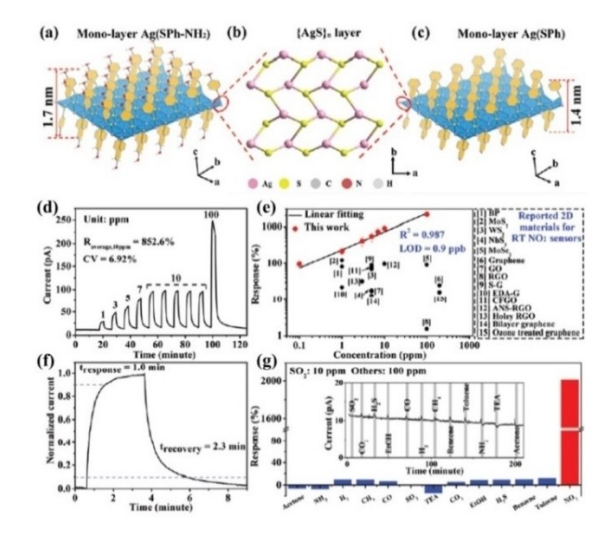


**Figure 32.** a, c) Monolayer structures in Ag(SPh $-NH_2$ ) and Ag(SPh). b) Inorganic AgS layer in Ag(SPh $-NH_2$ ) and Ag(SPh). Hydrogen atoms are omitted for clarity. d) Response-recovery curve of the Ag(SPh $-NH_2$ ) thin film under different concentrations of NO $_2$  at RT. e) Linear log-log plot of response vs. concentration and a comparison with reported 2D chemiresistive sensing materials working at RT. f) Normalized response-recovery curve to NO $_2$  under a concentration of 10 ppm. g) Sensitivities to 13 different gases; inset is the real-time measurement. [47] Copyright 2020 Royal Society Chemistry.





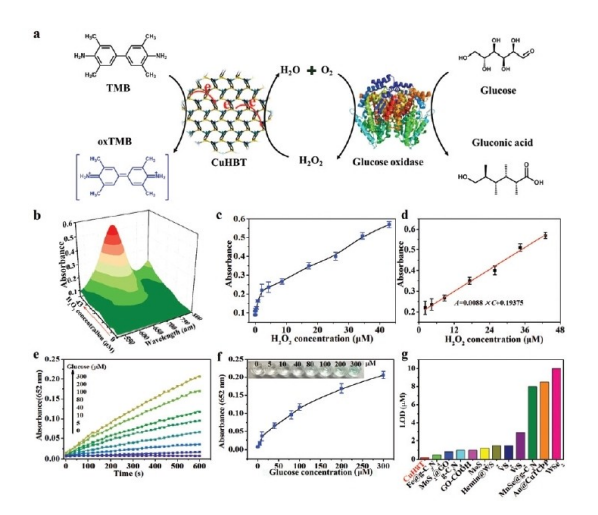


Figure 33. Detection of  $H_2O_2$  and glucose by 2D CuHT. a) Schematic illustration of colorimetric detection of glucose. b) UV/Vis absorption spectra of the detecting  $H_2O_2$  by a peroxidase mimic of 2D CuHT. c) and d) A dose-response curve for  $H_2O_2$  detection using CuHT. e) Time-course dependent absorbance changes under different concentration of glucose at 652 nm. f) A dose-response curve for glucose detection using CuHBT; The inset shows the photograph of the colored products with different concentrations of glucose. g) Comparison of the limit of detection of CuHT and other reported 2D materials. (48) Copyright 2019 Royal Society Chemistry.

#### 5. Conclusion and Prospects

The incorporation of organic functional groups into inorganic lattices at the molecular level makes it easier to introduce new properties into OMC materials. At present, most of the materials used for device preparation and performance exploration are thick nanosheets with a thickness of tens to hundreds of nanometers. Research on single-layer or few-layers OMCs is still in its infancy. However, the properties of OMCs should be largely different from those of their nanosheet precursors. They have great potential for applications different from those involving traditional 2D materials.

Although advances have been achieved in recent years, research on OMCs is still in its infancy. The challenges are as follows: 1) Only a few coinage-metal-based OMCs have been reported. Due to the limitation of valence state equilibrium and coordination configuration, the preparation of OMCs with other metals is still a great challenge. 2) The difficulty of obtaining single-crystal structures hinders exploration of the structure-performance relationship, and hence, the accompanying application potential is limited. Nevertheless, some advanced crystal structure analysis methods, such as 3D ED and smSFX, have been used to analyze the structures and the required crystal size decreases from large bulk single crystals to microcrystals. However, these methods require the use of expensive instruments and complicated techniques, which is why they have not been widely adopted. At present, only a few structures have been reported, and most of them are still resolved by powder diffraction. Methods to obtain crystals large enough for single-crystal data collection remain to be explored. 3) The inorganic layers are separated by the organic layers to form a particular multi-quantum-well structure. The thickness of the inorganic and organic layers will affect the width and depth of the quantum well, thus regulating the performance. However, the preparation of structures with controllable thickness of the inorganic layer and the organic layer is still a great challenge. 4) Although the methods of producing single-layer or few-layered OMCs have been reported in literature, the morphology and thickness of the products are not uniform. Large-scale and controllable preparation of monolayer or few-layered OMCs is difficult. 5) The OMCs exhibit excellent photoelectric properties but most of the devices reported so far are based on thick films or bulk materials. The small lateral size of the nanosheets impedes the fabrication of devices. Thus the preparation of single- or few-layered nanosheets with large lateral sizes is imperative. 6) The reported methods for obtaining few-layered OMCs mainly focus on traditional methods. Compared with inorganic two-dimensional materials, research on this system is scarce. 7) The selection of the appropriate precursor for the controllable synthesis of monolayer OMCs remains a great challenge. Much more effort is needed to find an optimal way to achieve the controllable preparation of monolayers with a high yield.

With the development of diffraction techniques, synthetic methods, and preparations, the above challenges will be overcome in the future. Benefitting from coordination chemistry, OMCs are capable of self-assembling at the molecular level. From the perspective of design, OMCs should be endowed with following features: 1) These materials still have much designability; it should be possible to extend organic chains to infinity to achieve the properties of monolayer structures in bulk materials. Meanwhile, the thickness of the inorganic layer, as the carrier transport layer, can also be regulated. 2) Under the modification of organic functional groups, OMCs are expected to show layer-dependent properties similar to those of other 2D materials, and relevant studies are urgently needed. 3) Due to the existence of ordered functional organic molecules, the types and the strength of interaction between the two materials can be regulated, making the co-assembly of different OMCs easier. Thus new performance is expected. 4) The organic functional groups arranged in an orderly manner and in long-range on the surface make OMCs a very desirable new material in surface chemistry, which can further be used as substrates for epitaxial growth of other crystalline films or for the direct covalent modification of other functional materials. 5) The doping of other elements will bring more novel properties to these materials. These studies have not yet been carried out.

The purposeful and rational design and effective synthesis of OMCs with specific structure and properties is still in their infancy, and there is still a long way to go for practical application. More new practical OMCs will be explored by taking the advantages of their unique structures. Additionally, a method that can be used to obtain few-layered OMCs with good crystallinity, and uniformly controlled size and thickness is urgently needed. The related issues have not been fully studied so far, but they may be





solved in the future with more researchers participating in this field, which would undoubtedly promote vivid growth of this research field.

### Acknowledgements

This work supported by the National Natural Science Foundation of China (91961115, 22171263, 21975254, 22175176, 21822109). The NSF of Fujian (2021 J02017, 2020 J01109). Youth Innovation Promotion Association CAS (2018342). Fujian Science & Technology Innovation Laboratory for Optoelectronic Information of China (2021ZR101). Scientific Instrument Developing Project of the Chinese Academy of Sciences (YJKYQ20210024).

## **Conflict of Interest**

The authors declare no conflict of interest.

**Keywords:** 2D Materials • Functional Motifs • OMCs • Organic Metal Chalcogenides • Synthetic Strategies

- a) C. Tan, X. Cao, X. J. Wu, Q. He, J. Yang, X. Zhang, J. Chen, W. Zhao, S. Han, G. H. Nam, M. Sindoro, H. Zhang, Chem. Rev. 2017, 117, 6225–6331; b) C. Tan, Z. Lai, H. Zhang, Adv. Mater. 2017, 29, 1701392; c) Z. Li, D. Li, H. Wang, P. Chen, L. Pi, X. Zhou, T. Zhai, Small Methods 2021, 5, 2100567; d) D. Ouyang, X. Tong, S. Liu, J. Wang, Y. Zhao, R. Liu, X. Zhao, N. Zhang, F. Cao, Y. Liu, Y. Li, L. Li, T. Zhai, Adv. Funct. Mater. 2022, 32, 2113052; e) W. Xue, Q. Jiang, F. Wang, R. He, R. Pang, H. Yang, P. Wang, R. Yang, Z. Zhong, T. Zhai, X. Xu, Small 2022, 18, 2105599.
- [2] a) D. Voiry, A. Goswami, R. Kappera, C. Silva Cde, D. Kaplan, T. Fujita, M. Chen, T. Asefa, M. Chhowalla, *Nat. Chem.* 2015, 7, 45–49; b) Q. Tang, D.-E. Jiang, *Chem. Mater.* 2015, 27, 3743–3748; c) Y. Jiang, T. Sun, X. Xie, W. Jiang, J. Li, B. Tian, C. Su, *ChemSusChem* 2019, 12, 1368–1373; d) X.-M. Jiang, S. Deng, M.-H. Whangbo, G.-C. Guo, *Natl. Sci. Rev.* 2022, DOI: 10.1093/nsr/nwac017.
- [3] Y. Li, X. Jiang, Z. Fu, Q. Huang, G. E. Wang, W. H. Deng, C. Wang, Z. Li, W. Yin, B. Chen, G. Xu, Nat. Commun. 2020, 11, 261.
- [4] B. Trang, M. Yeung, D. C. Popple, E. A. Schriber, M. A. Brady, T. R. Kuykendall, J. N. Hohman, J. Am. Chem. Soc. 2018, 140, 13892–13903.
- [5] X. Deng, S.-L. Zheng, Y.-H. Zhong, J. Hu, L.-H. Chung, J. He, Coord. Chem. Rev. 2022, 450, 214235.
- [6] Ian G. Dance, Keith J. Fisher, R. M. H. Banda, S. Marcia L, Inorg. Chem. 1991, 30, 183–187.
- [7] W. Su, M. Hong, J. Weng, R. Cao, S. Lu, Angew. Chem. Int. Ed. 2000, 39, 2911–2914; Angew. Chem. 2000, 112, 3033–3036.
- [8] H. L. Cuthbert, Andrew I. Wallbank, Nicholas J. Taylor, John F. Corrigan, Z. Anorg. Allg. Chem. 2002, 628, 2483–2488.
- [9] K. H. Low, V. A. Roy, S. S. Chui, S. L. Chan, C. M. Che, Chem. Commun. 2010, 46, 7328–7330.
- [10] M. S. A. Begum, U. Flörke, G. Henkel, *Inorg. Chim. Acta* 2010, 363, 2144–2148.
- [11] X.-P. Kang, Y.-S. Hu, L.-H. Zhu, Z. An, *Inorg. Chem. Commun.* 2013, 29, 169–171.

- [12] L. Ma, W. Chen, G. Schatte, W. Wang, A. G. Joly, Y. Huang, R. Sammynaiken, M. Hossu, J. Mater. Chem. C 2014, 2, 4239– 4246.
- [13] C. Lavenn, N. Guillou, M. Monge, D. Podbevsek, G. Ledoux, A. Fateeva, A. Demessence, *Chem. Commun.* 2016, 52, 9063– 9066.
- [14] O. Veselska, D. Podbevsek, G. Ledoux, A. Fateeva, A. Demessence, Chem. Commun. 2017, 53, 12225–12228.
- [15] O. Veselska, L. Cai, D. Podbevsek, G. Ledoux, N. Guillou, G. Pilet, A. Fateeva, A. Demessence, *Inorg. Chem.* 2018, 57, 2736–2743.
- [16] A. Pathak, J. W. Shen, M. Usman, L. F. Wei, S. Mendiratta, Y. S. Chang, B. Sainbileg, C. M. Ngue, R. S. Chen, M. Hayashi, T. T. Luo, F. R. Chen, K. H. Chen, T. W. Tseng, L. C. Chen, K. L. Lu, *Nat. Commun.* 2019, 10, 1721.
- [17] Z. Wu, Q. Yao, Z. Liu, H. Xu, P. Guo, L. Liu, Y. Han, K. Zhang, Z. Lu, X. Li, J. Zhang, J. Xie, Adv. Mater. 2021, 33, 2006459.
- [18] E. A. Schriber, D. W. Paley, R. Bolotovsky, D. J. Rosenberg, R. G. Sierra, A. Aquila, D. Mendez, F. Poitevin, J. P. Blaschke, A. Bhowmick, R. P. Kelly, M. Hunter, B. Hayes, D. C. Popple, M. Yeung, C. Pareja-Rivera, S. Lisova, K. Tono, M. Sugahara, S. Owada, T. Kuykendall, K. Yao, P. J. Schuck, D. Solis-Ibarra, N. K. Sauter, A. S. Brewster, J. N. Hohman, *Nature* 2022, 601, 360–365.
- [19] a) X. Huang, J. Li, J. Am. Chem. Soc. 2000, 122, 8789–8790;
   b) X. Huang, J. Li, J. Am. Chem. Soc. 2007, 129, 3157–3162.
- [20] O. Veselska, L. Okhrimenko, N. Guillou, D. Podbevšek, G. Ledoux, C. Dujardin, M. Monge, D. M. Chevrier, R. Yang, P. Zhang, A. Fateeva, A. Demessence, J. Mater. Chem. C 2017, 5, 9843–9848.
- [21] a) H. Nie, M. Li, Y. Hao, X. Wang, S. Gao, P. Wang, B. Ju, S. X.-A. Zhang, RSC Adv. 2014, 4, 50521–50528; b) S. Zhang, Y. Yu, S. Xu, J. Liu, M. Liu, H. Su, Y. Hao, M. Li, S. X. A. Zhang, ChemNanoMat 2021, 7, 270–276.
- [22] O. Veselska, A. Demessence, Coord. Chem. Rev. 2018, 355, 240–270.
- [23] D. V. P. Massote, M. S. C. Mazzoni, Appl. Phys. Lett. 2016, 109, 133104.
- [24] K. Yao, M. S. Collins, K. M. Nell, E. S. Barnard, N. J. Borys, T. Kuykendall, J. N. Hohman, P. J. Schuck, ACS Nano 2021, 15, 4085–4092.
- [25] a) E. A. Schriber, D. J. Rosenberg, R. P. Kelly, A. Ghodsi, J. N. Hohman, Front. Chem. 2021, 9, 593637; b) E. A. Schriber, D. C. Popple, M. Yeung, M. A. Brady, S. A. Corlett, J. N. Hohman, ACS Appl. Nano Mater. 2018, 1, 3498–3508.
- [26] W. Paritmongkol, T. Sakurada, W. S. Lee, R. Wan, P. Muller, W. A. Tisdale, J. Am. Chem. Soc. 2021, 143, 20256–20263.
- [27] L. Hu, Z. Zhang, M. Zhang, M. Y. Efremov, E. A. Olson, L. P. de la Rama, R. K. Kummamuru, L. H. Allen, *Langmuir* 2009, 25, 9585–9595.
- [28] a) L. Maserati, S. Pecorario, M. Prato, M. Caironi, J. Phys. Chem. C 2020, 124, 22845–22852; b) L. Maserati, M. Prato, S. Pecorario, B. Passarella, A. Perinot, A. A. Thomas, F. Melloni, D. Natali, M. Caironi, Nanoscale 2021, 13, 233–241.
- [29] Y.-Z. Li, Z.-H. Fu, G. Xu, Coord. Chem. Rev. 2019, 388, 79– 106.
- [30] H. Nie, M. Li, Y. Hao, X. Wang, S. Gao, B. Yang, M. Gu, L. Sun, S. X. Zhang, J. Colloid Interface Sci. 2014, 434, 104–112.
- [31] H. Nie, M. Li, Y. Hao, X. Wang, S. X.-A. Zhang, Chem. Sci. 2013, 4, 1852–1857.
- [32] J. Yang, Y. Li, L. Guo, B. Qiu, Z. Lin, Anal. Chem. 2021, 93, 11010–11018.
- [33] Y. Hao, C. Dai, L. Yu, S. Li, Y. Yu, B. Ju, M. Li, S. X.-A. Zhang, CrystEngComm 2018, 20, 181–188.
- [34] C. Dai, S. Xu, Y. Yu, M. Li, S. X.-A. Zhang, J. Phys. Chem. C 2020, 124, 24400–24407.





- [35] Y. Hao, L. Yu, C. Dai, S. Li, Y. Yu, B. Ju, M. Li, S. X. Zhang, Chem. Eur. J. 2017, 23, 13525–13532.
- [36] Y. Wen, G. E. Wang, X. Jiang, X. Ye, W. Li, G. Xu, Angew. Chem. Int. Ed. 2021, 60, 19710–19714; Angew. Chem. 2021, 133, 19862–19866.
- [37] L. Maserati, S. Refaely-Abramson, C. Kastl, C. T. Chen, N. J. Borys, C. N. Eisler, M. S. Collins, T. E. Smidt, E. S. Barnard, M. Strasbourg, E. A. Schriber, B. Shevitski, K. Yao, J. N. Hohman, P. J. Schuck, S. Aloni, J. B. Neaton, A. M. Schwartzberg, *Mater. Horiz.* 2021, 8, 197–208.
- [38] Q.-Q. Huang, Y.-Z. Li, Z. Zheng, X.-M. Jiang, S.-S. Sun, H.-J. Jiang, W.-H. Deng, G.-E. Wang, T.-Y. Zhai, M.-D. Li, G. Xu, CCS Chem. 2020, 2, 655–662.
- [39] a) Sang-Ho Cha, Jong-Uk Kim, Ki-Hyun Kim, J.-C. Lee, Chem. Mater. 2007, 19, 6297–6303; b) Sang-Ho Cha, Ki-Hyun Kim, Jong-Uk Kim, Won-Ki Lee, J.-C. Lee, J. Phys. Chem. C 2008, 112, 13862–13868.
- [40] O. Veselska, C. Dessal, S. Melizi, N. Guillou, D. Podbevsek, G. Ledoux, E. Elkaim, A. Fateeva, A. Demessence, *Inorg. Chem.* 2019, 58, 99–105.
- [41] J. Troyano, O. Castillo, J. I. Martínez, V. Fernández-Moreira, Y. Ballesteros, D. Maspoch, F. Zamora, S. Delgado, Adv. Funct. Mater. 2018, 28, 1704040.
- [42] a) L. M. Cavinato, E. Fresta, S. Ferrara, R. D. Costa, Adv. Energy Mater. 2021, 11, 2100520; b) B. Kan, J. Zhang, F. Liu, X. Wan, C. Li, X. Ke, Y. Wang, H. Feng, Y. Zhang, G. Long,

- R. H. Friend, A. A. Bakulin, Y. Chen, *Adv. Mater.* **2018**, *30*, 1704904; c) H. Chen, H. Lai, Z. Chen, Y. Zhu, H. Wang, L. Han, Y. Zhang, F. He, *Angew. Chem. Int. Ed.* **2021**, *60*, 3238–3246; *Angew. Chem.* **2021**, *133*, 3275–3283.
- [43] G. Xing, Y. Li, Z. Feng, D. J. Singh, F. Pauly, ACS Appl. Mater. Interfaces 2020, 12, 53841–53851.
- [44] K. Li, L. Xu, Z. Li, Y. Wang, J. Wang, X. Qi, Q. Li, H. Wang, Nano Energy 2021, 84, 105902.
- [45] a) M. B. Kale, R. A. Borse, A. Gomaa Abdelkader Mohamed, Y. Wang, Adv. Funct. Mater. 2021, 31, 2101313; b) T. Ioroi, Z. Siroma, S. I. Yamazaki, K. Yasuda, Adv. Energy Mater. 2018, 9, 1801284; c) X. Jin, T.-H. Gu, K.-G. Lee, M. J. Kim, M. S. Islam, S.-J. Hwang, Coord. Chem. Rev. 2020, 415, 213280.
- [46] A. N. Yang, J. T. Lin, C. T. Li, ACS Appl. Mater. Interfaces 2021, 13, 8435–8444.
- [47] H. Jiang, L. Cao, Y. Li, W. Li, X. Ye, W. Deng, X. Jiang, G. Wang, G. Xu, Chem. Commun. 2020, 56, 5366–5369.
- [48] Y. Li, J. Shu, Q. Huang, K. Chiranjeevulu, P. N. Kumar, G. E. Wang, W. H. Deng, D. Tang, G. Xu, *Chem. Commun.* 2019, 55, 10444–10447.

Manuscript received: February 28, 2022 Accepted manuscript online: April 20, 2022 Version of record online:





# **Minireviews**

### 2D Materials

G.-E Wang, S. Luo, T. Di, Z. Fu, G. Xu\* \_\_\_\_\_\_\_\_\_ e202203151

Layered Organic Metal Chalcogenides (OMCs): From Bulk to Two-Dimensional Materials



With metal chalcogenide layers covalently anchored by long-range ordered organic functional motifs, organic metal chalcogenides are a type of newly emerging 2D materials, which are exquisitely desired but impossible to realize by traditional methods for the synthesis of

2D materials. This Minireview gives a perspective on the structural design of bulk precursors, exfoliation methods, applications, and discusses research directions based on recently published work.